Drug Design, Development and Therapy

Dovepress

open access to scientific and medical research

Open Access Full Text Article

ORIGINAL RESEARCH

# Network Pharmacology-Based Strategy Combined with Molecular Docking and in vitro Validation Study to Explore the Underlying Mechanism of Huo Luo Xiao Ling Dan in Treating Atherosclerosis

Taoli Sun[1], Wenjuan Quan[1], Sha Peng[1], Dongmei Yang[2], Jiaqin Liu[3], Chaoping He[1], Yu Chen[2], Bo Hu[2], Qinhui Tuo[2,4]

[1]School of Pharmacy, Hunan University of Chinese Medicine, Changsha, 410208, People's Republic of China; [2]School of Medicine, Hunan University of Chinese Medicine, Changsha, 410208, People's Republic of China; [3]Department of Pharmacy, the Second Xiangya Hospital, Central South University, Changsha, Hunan, 410011, People's Republic of China; [4]The First hospital of Hunan University of Chinese Medicine, Changsha, 410007, People's Republic of China

Correspondence: Qinhui Tuo, School of Medicine, Hunan University of Chinese Medicine, Changsha, 410208, People's Republic of China, Tel +86-18874089105, Email qhtuo@aliyun.com

**Background:** Huo Luo Xiao Ling Dan (HLXLD), a famous Traditional Chinese Medicine (TCM) classical formula, possesses anti-atherosclerosis (AS) activity. However, the underlying molecular mechanisms remain obscure.

**Aim:** The network pharmacology approach, molecular docking strategy, and in vitro validation experiment were performed to explore the potential active compounds, key targets, main signaling pathways, and underlying molecular mechanisms of HLXLD in treating AS.

**Methods:** Several public databases were used to search for active components and targets of HLXLD, as well as AS-related targets. Crucial bioactive ingredients, potential targets, and signaling pathways were acquired through bioinformatics analysis. Subsequently, the molecular docking strategy and molecular dynamics simulation were carried out to predict the affinity and stability of active compounds and key targets. In vitro cell experiment was performed to verify the findings from bioinformatics analysis.

**Results:** A total of 108 candidate compounds and 321 predicted target genes were screened. Bioinformatics analysis suggested that quercetin, dihydrotanshinone I, pelargonidin, luteolin, guggulsterone, and β-sitosterol may be the main ingredients. STAT3, HSP90AA1, TP53, and AKT1 could be the key targets. MAPK signaling pathway might play an important role in HLXLD against AS. Molecular docking and molecular dynamics simulation results suggested that the active compounds bound well and stably to their targets. Cell experiments showed that the intracellular accumulation of lipid and increased secretory of TNF-α, IL-1β, and MCP-1 in ox-LDL treated RAW264.7 cells, which can be significantly suppressed by pretreating with dihydrotanshinone I. The up-regulation of STAT3, ERK, JNK, and p38 phosphorylation induced by ox-LDL can be inhibited by pretreating with dihydrotanshinone I.

**Conclusion:** Our findings comprehensively demonstrated the active compounds, key targets, main signaling pathways, and underlying molecular mechanisms of HLXLD in treating AS. These findings would provide a scientific basis for the study of the complex mechanisms underlying disease and drug action.

**Keywords:** Huo Luo Xiao Ling Dan, atherosclerosis, network pharmacology, molecular docking, molecular dynamics simulation, dihydrotanshinone I, STAT3, MAPK signaling pathway

## Introduction

Atherosclerosis (AS), a lipid-driven chronic inflammatory vascular disease characterized by progressive thickening of the blood vessel wall, is one of the main causes of death from cardiovascular disease. The pathogenesis of AS involved a variety of possible mechanisms, including lipid infiltrations, injury responses, inflammatory responses, immunological responses, and hemodynamic effects.[1–3] AS can be induced by long-term elevated blood lipids and cause a variety of

Received: 22 January 2022
Accepted: 13 May 2022
Published: 30 May 2022

cardiovascular-related complications, such as thrombosis, ischemia, and angina pectoris.[4] Therefore, effective prevention and treatment against AS are of great significance in the prevention of certain cardiovascular diseases.[5] Most individuals with AS need to be treated with lipid-lowering drugs (such as statins).[4] However, statins have many inevitable side effects, for example, liver/kidney dysfunction and rhabdomyolysis.[6] Moreover, new options now exist for the prevention of AS that are not optimized for statin therapy.[7]

Traditional Chinese Medicine (TCM) is a unique health resource in China and has been applied to human beings for more than two thousand years. Recent studies show that TCM has the potential to prevent and treat a variety of diseases, such as COVID-19,[8] cancer,[9] ischaemic stroke,[10] primary dysmenorrhea,[11] and mild active ulcerative colitis.[12] In the treatment of AS, TCM shows unique advantages, including the overall regulatory function of the body and the little toxic and side effects.[13–15]

Huo Luo Xiao Ling Dan (HLXLD) is a classic formula in the medical records of Yi-Xue-Zhong-Zhong-Can-Xi-Lu by Zhang Xichun,[16] consisting of *Angelica sinensis, Salvia miltiorrhiza, Commiphora myrrha*, and *Boswellia sacra* (the detail information about the formula of HLXLD was listed in Table 1).[17] In recent years, increasing evidence suggests that HLXLD may be effective in the treatment of AS. HLXLD up-regulates the protective factor TGF-β to inhibit the immune-inflammatory response in ApoE knock-out mice with early AS.[18] HLXLD treatment can decrease the values of TC, TG, HDL, TC/HDL, and TG/HDL in serum, indicating the potential to treat AS.[19] Moreover, studies have shown that the active ingredients derived from HLXLD, such as quercetin,[20] luteolin,[21] dihydrotanshinone I,[22] β-sitosterol[23] and tanshinone IIA,[24] exhibit potent pharmacological activities against AS based on individual single compounds of HLXLD. Like other TCM, HLXLD has a complex mechanism involving many complicated relationships between components and targets, targets and diseases, targets and pathways in the treatment of certain diseases.

A modern research strategy combining network science, computer science, mathematics, and network pharmacology has been widely used in TCM research. This research strategy can help to clarify the action mechanisms and pathways of TCM from the aspects of molecular level or molecular network regulation, and screen out active ingredients or disease targets from a large number of data.[25,26] Additionally, molecular docking technology is a theoretical simulation method for studying the intermolecular interactions (such as small-molecule ligands and biomacromolecules), and predicting their binding modes and affinity.[27,28] The combination of network pharmacology prediction and molecular docking-based strategy has been applied in a large number of studies to discover the potential pharmacological mechanism of TCM. For instance, Liu et al identified 95 active compounds and 265 predicted targets in Bu Yang Huan Wu decoction by network pharmacology analysis and revealed that the mechanism of Bu Yang Huan Wu decoction in treating AS is related to inflammation and apoptosis pathways. In the early stage, we have conducted a network pharmacology approach to identify the active ingredients of Huai Hua San and explore the mechanisms underlying the treatment of ulcerative colitis.[29]

In the present study, as shown in Figure 1, we adopted the method of network pharmacology to find the active compounds and anti-AS targets of HLXLD by constructing a multi-dimensional network diagram. Subsequently, Gene Ontology (GO) and Kyoto Encyclopedia of Genes and Genomes (KEGG) functional enrichment analysis combined with molecular docking and cell verification experiments were carried out to investigate the complex effects of botanical drugs on the prescriptions. These findings may provide a scientific basis and ideas for follow-up research.

**Table 1** Detailed Information About the Formula of HLXLD

| Herbal Components | Chinese Name | Scientific Name | Family | Part(s) of Plant Used | Quanitity in HLXLD |
|---|---|---|---|---|---|
| *Angelica sinensis* | Danggui | Angelica sinensis (Oliv.) Diels | Apiaceae | root | 25% |
| *Salvia miltiorrhiza* | Dansheng | Salvia miltiorrhiza Bunge | Lamiaceae | rhizome, root | 25% |
| *Commiphora myrrha* | Moyao | Commiphora myrrha (T.Nees) Engl. | Burseraceae | resin | 25% |
| *Boswellia sacra* | Ruxiang | Boswellia sacra Flück. | Burseraceae | resin | 25% |

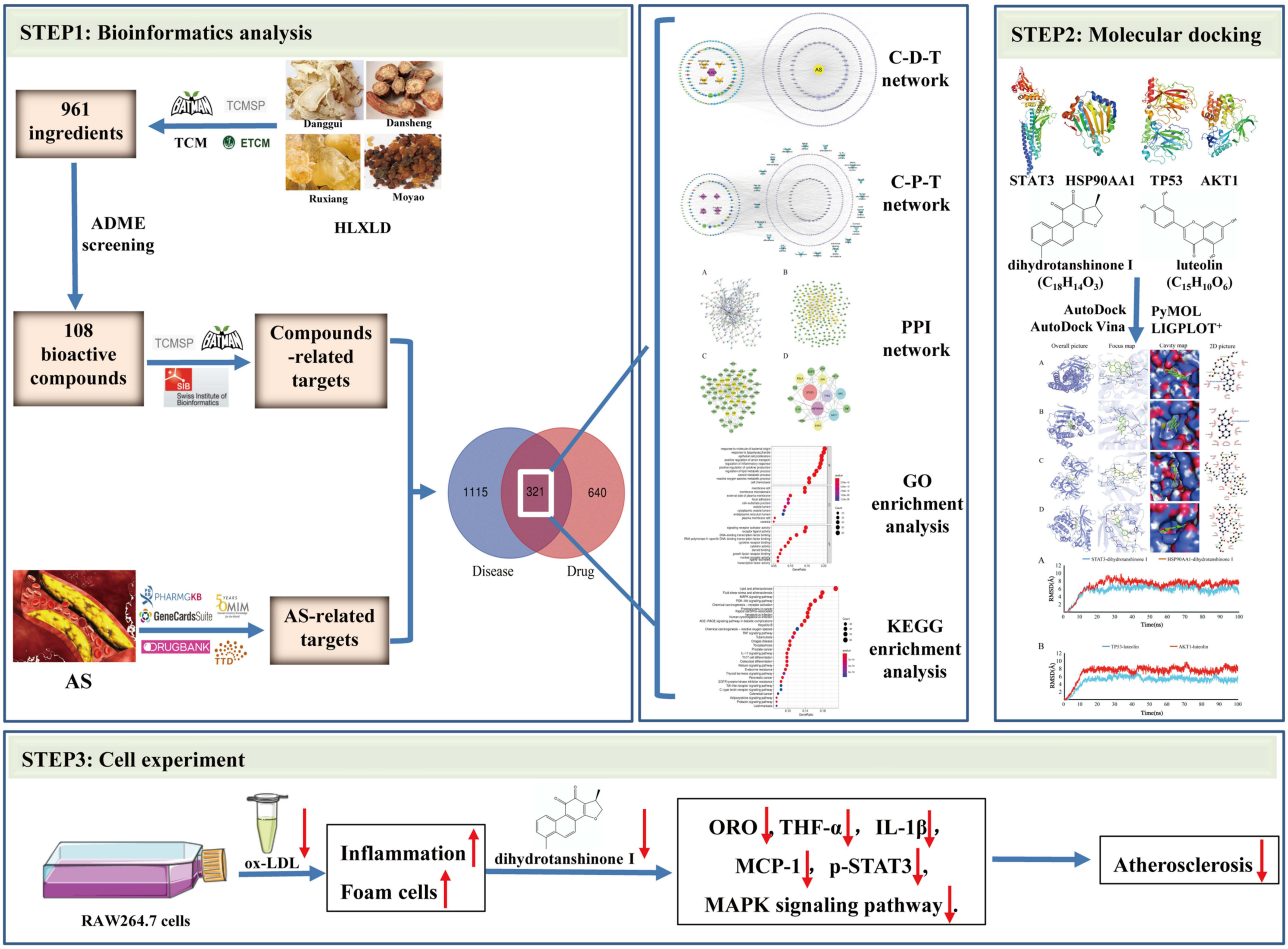


**Figure 1** Schematic representation of the proposed mechanism in HLXLD against AS. Network pharmacology was performed to identify the active compounds and key targets of HLXLD against AS. Molecular docking and molecular dynamics simulation were conducted to predict the interaction and connection stability between active components and candidate targets. Cell experiments confirmed that lipid accumulation, inflammation and MAPK signaling pathway were alleviated by candidate compound dihydrotanshinone I in ox-LDL-induced RAW264.7 cells.

# Materials and Methods

## Data Preparation

### Active Ingredients of HLXLD

The compounds of HLXLD were searched from four public databases including Traditional Chinese Medicine Systems Pharmacology Database and Analysis Platform (TCMSP, https://tcmsp-e.com/), The Encyclopedia of Traditional Chinese Medicine (ETCM, http://www.tcmip.cn/ETCM/index.php/Home/Index/index.html), Bioinformation Analysis Tool for Molecular mechanism of Traditional Chinese Medicine (BATMAN-TCM, http://bionet.ncpsb.org.cn/batman-tcm/) and Traditional Chinese Medicine Database@Taiwan (TCM, Database@Taiwan, http://tcm.cmu.edu.tw/zh-tw/review.php?menuid=3). The OB (oral bioavailability) and DL (drug-likeness) values of compounds were obtained from TCMSP, and only compounds meeting the screening criteria of OB >30% and DL ≥ 0.18 were retained for further research.

### Targets Prediction of HLXLD and as

The study was performed in accordance with good clinical practice standards and the tenets of the Declaration of Helsinki 2002, and approved by the clinical research ethics committee in the Second Xiangya Hospital of Central South University (No. 2021–248). The approval certificate was provided in the supporting information. Targets prediction of HLXLD obtained from three public databases, including TCMSP, BATMAN-TCM (score cutoff was set to 20, and adjusted P-value was set to 0.05) and the webtool of SwissTargetPrediction (SwissTargetPrediction, http://www.swissstargetprediction.ch/, Prob value >0). We selected "Homo sapiens" as a species. The chemical information was obtained

from the PubChem database (PubChem, https://pubchem.ncbi.nlm.nih.gov/). The protein target names were converted to their corresponding official gene symbols by the UniProt database (https://www.uniprot.org/). Besides, targets of AS were explored by the keyword of "atherosclerosis" from five public databases, including GeneCards: The human gene database (https://www.genecards.org/, Ver. 5.7, Relevance score ≥1), Online Mendelian Inheritance in Man (OMIM, https://omim.org/, Updated September 4th, 2021), PharmGKB (https://www.pharmgkb.org/), Therapeutic Target Database (TTD, http://db.idrblab.net/ttd/, Updated September 29th, 2021), and DrugBank (https://go.drugbank.com/). Only "Homo sapiens" proteins linked to atherosclerosis were selected. Venn diagram of disease targets in five databases were drawn using R software. The Venn diagram of common targets of HLXLD and AS were drawn on the website of http://bioinformatics.psb.ugent.be/webtools/Venn/.

## Bioinformatics Analysis

### Protein–Protein Interaction (PPI) Network Construction

PPI network of common targets of HLXLD and AS was constructed using the functional protein association networks database (STRING, https://cn.string-db.org/), with species limited to "Homo sapiens". The minimum required interaction score was set to 0.98, and the independent target protein nodes were hidden. To obtain the potential core target network, the PPI network was visualized by Cytoscape 3.8.2.

Core targets were screened out by calculating six topological parameters of nodes, including betweenness centrality (BC), closeness centrality (CC), degree centrality (DC), eigenvector centrality (EC), network centrality (NC), and local average connectivity (LAC), through CytoNCA plugin in Cytoscape software, which can be utilized to quantitatively assess the calculation results, evaluate the accuracy by statistical measures and integrate biological data with topological data to detect specific nodes. After calculating six parameters using the CytoNCA plugin, only nodes with all six parameters higher than the corresponding median values were retained to further construct the core PPI network.

## Enrichment Analysis

After converting the common official gene symbols of HLXLD and AS to Entrez ID by R 4.1.1 software, GO and KEGG pathway enrichment analyses were carried out using R 4.1.1 software with related R packages (colorspace, stringi, DOSE, clusterProfiler, ggplot2, enrichplot, pathview, BiocManager, and org.Hs.eg.db). $Q$ values <0.05 were considered statistically significant and retained.

## Network Construction

To illustrate the relationship between botanical drugs and compounds, diseases and targets, as well as targets and signal pathways, the four botanical drugs, candidate active compounds, common target genes, disease name and top 20 pathways were introduced into Cytoscape 3.8.2 to construct a network of Compounds-Disease-Targets (C-D-T) and Compounds-Pathway-Targets (C-P-T) network.

## Molecular Docking

The compounds with the highest degree in the C-D-T network and target proteins with the highest degree in the core network were chosen to conduct molecular docking with AutoDock 1.5.6 Vina. The process of the molecular docking experiment was as follows:

First, receptor and ligand preparation of 3D structure: The 3D structural receptors were downloaded from Protein Data Bank (PDB, https://www.rcsb.org/) meeting the standard as far as possible: Organism(s) from "Homo sapiens", no mutation(s), with higher resolution and containing small-molecule ligand(s). The 2D structural ligands were downloaded from the PubChem database (https://pubchem.ncbi.nlm.nih.gov/), and then imported into Chem3D software to obtain the 3D structure of ligands. The receptor was saved in pdb format, and the ligand was saved in mol2 format.

Second, receptor and ligand preparation of pdbqt format: The macromolecule receptor was opened in Pymol software to remove water molecules, co-crystallized ligands, and ions. Subsequently, the macromolecule receptor was inputted into AutoDockTools 1.5.6 to add hydrogens and Kollman partial charges, and saved in pdbqt format. Then, the ligand was opened in AutoDockTools 1.5.6 and saved in pdbqt format.

Third, prediction of mating pockets of macromolecule receptor: The pdbqt format of the receptor was imported to AutoDockTools 1.5.6 to construct mating pockets of docking. Using the self-carrying molecules surrounding the protein crystal structure as the geometric center, a box with the largest range was formed. Spacing (angstrom) was set to 1, energy_range was set to 5, num_modes was set to 20, the numbers of points in the mating box (centre_x, centre_y, centre_z), and the size of the mating box (size_x, size_y, size_z) were set on the macromolecule and set to keep the protein completely covered by mating box, respectively. These parameters were saved in a configuration (config) file of each protein mating box for further docking by Vina.

Docking and visualization: Molecular docking and calculation of docking affinity were operated with Vina software. During the process, pdbqt files of protein and ligand were also used in addition to the config file containing the information of the mating box. The program performed a conformational search for the ligand in the box range and finally scored according to their conformation, orientation, position and energy of the ligand by Vina. After Vina finished running, the binding affinity score between the macromolecule receptor and small-molecule ligand was output as log.txt files. The best combination mode of receptor and ligand was presented at the first line in log.txt with the lowest docking binding free energy. The interaction between receptor and ligand was visualized and hydrogen bonds were displayed by Pymol (3D) and LigPlus (2D).

## Molecular Dynamics Simulation

After docking, the molecular dynamics (MD) simulation strategy was carried out to simulate the binding stability of the receptor and ligand. The entire system added AmberFF99SB and gaff force field parameters to proteins and molecules to set the force fields of carbon atoms and oxygen atoms with different bond angles. Subsequently, with the protein as the center, a 1-nm cubic water box and $Na^+$ were added to make the system stable. In the end, MD simulations were performed.

The MD simulation process was as follows: 1) Two-step energy minimization. We firstly limited the protein, minimized the energy of water molecules, and then released the protein, thereby minimizing the energy of the entire system. In the first energy minimization, a total of 5000 cycles were used, and the steepest descent method was used for 1500 cycles. The second energy was minimized for a total of 5000 cycles, and the steepest descent method was firstly used to make 2000 cycles. 2) System balance. The system is heated from 0°C to 100°C, and the Langevin temperature control method was used to balance 100 ps. Then, we proceeded to the boost balance process, during which a total of 100 ps were balanced, and the isotropic Berendsen voltage control method was used. 3) Dynamic simulation. In this dynamic process, a constant temperature of 100°C was used to perform a molecular dynamics simulation of the overall system. The temperature and voltage control methods were the same as in the previous stage. The cutoff distance between van der Waals energy and short-range electrostatic energy was 10 Å, and the Particle-Mesh-Ewald (PME) method was used to calculate the long-range electrostatic energy.

In the process of molecular dynamics, the human body temperature was used for the system. The molecular dynamics time was controlled at 100 ns, and the RMSD value of the complex system was monitored in real time until the project goal was reached. Subsequently, the average structure of the protein-molecule meeting the expectations was taken out for subsequent binding mode analysis.

## In vitro Validation

### Cell Culture

The mouse mononuclear macrophage leukemia cell line (RAW264.7) was purchased from Beijing Beina Chuanglian Institute of Biotechnology (Beijing, China) and cultured using Dulbecco's Minimum Essential Medium (DMEM) medium containing 10% fetal bovine serum (FBS), 100μg/mL streptomycin, and 100U/mL penicillin. Cells were incubated at 37°C in a humidified atmosphere of 5% $CO_2$ and 95% air.

### Oil Red O Staining

RAW264.7 cells were cultured in 6-well culture plates with sterile coverslips to assess foam cell formation. The cells were pretreated with dihydrotanshinone I with a concentration of 10, 100, 1000 nM for one hour, then treated with 50 μg/

mL ox-LDL for 24 h. After treatment, the cells were washed three times with PBS, fixed with 50% isopropanol for one minute, and stained with oil red O staining solution for 10 min, followed by discarding the dye solution and washing it three times. Foam cells were photographed under a microscope and analyzed using an image analysis system.

### Cytokine Enzyme-Linked Immunosorbent Assay (ELISA)

RAW264.7 cells were cultured in 6-well culture plates and pretreated with dihydrotanshinone I with a concentration of 10, 100, 1000 nM for one hour, then treated with 50 μg/mL ox-LDL for 24 h. The levels of TNF-α, IL-1β, and MCP-1 in cell supernatants were determined by an ELISA assay kit meeting the manufacturer's protocol. Quantitative determinations were performed in three independent experiments.

## Western Blot Analysis

Total cellular protein was collected by using a high-efficiency radio immunoprecipitation assay (RIPA) buffer with 0.1% PMSF (BOSTER Biological Technology; Wuhan, China) and the total protein concentration of each sample was determined using a BCA kit. The protein samples were separated by SDS-PAGE using 8–10% gradient gel. The separated protein on the gel was transferred onto 0.45 μm PVDF membranes. The expression of the target protein was normalized to GAPDH protein. Antibodies against p-STAT3 (#9145, Cell Signaling Technology, Danvers, MA, USA), STAT3 (#4904), p38 (#8690), and p-p38 (#4511) were purchased from Cell Signaling Technology (Danvers, MA, USA), and antibodies against ERK (ab17942), p-ERK (ab278538), JNK (ab199380) and p-JNK (ab124956) were purchased from Abcam (Cambridge, UK).

## Statistical Analysis

The results were presented as means ± S.E.M and data comparison of multiple groups was adopted using one-way ANOVA and Student-Newman-Keuls test. The results were considered statistically significant when the *P* value was less than 0.05.

# Results

## Potential Active Components in HLXLD

HLXLD is composed of *Angelica sinensis, Salvia miltiorrhiza, Commiphora myrrha*, and *Boswellia sacra*. After ADME screening (OB >30% and DL ≥0.18), a total of 108 potentially active compounds were retrieved from four databases (Table 2). Among them, six are from *Angelica sinensis*, 66 from *Salvia miltiorrhiza*, 29 from *Commiphora myrrha*, four from *Boswellia sacra*, and three (beta-sitosterol, stigmasterol, isoimperatorin) from two or more botanical drugs.

## Common Targets of HLXLD and AS

After the initial search from TCSMP, BATMAN-TCM, and SwissTargetPrediction, 6014 targets were predicted from 108 bioactive compounds in HLXLD. Subsequently, we removed duplicate values and converted protein names into gene symbols, thereby obtaining 961 targets (Supplement Table 1). Besides, 1463 AS-related targets were searched from five databases, including 1387 in GeneCards (Relevance score ≥1), 25 in PharmGkb, 24 in TTD, 26 in DrugBank, and one in OMIM. After we removed duplicate values, 1436 targets were obtained (Figure 2A, Supplement Table 1). Then, the 321 common targets of HLXLD and AS were achieved by R software for subsequent study (Figure 2B, Supplement Table 1).

## C-D-T Network Construction and Topological Network Analysis

To obtain a further understanding of the relationship between the 108 compounds and 321 intersection target genes on a system level, the C-D-T network with 429 nodes and 1754 edges was constructed by Cytoscape 3.8.2 (Figure 3). The turmeric V nodes represent four botanical drugs from HLXLD. The circular nodes of red, blue, green, and yellow stand for compounds from *Angelica sinensis, Salvia miltiorrhiza, Commiphora myrrha* and *Boswellia sacra*, respectively. The circular purple nodes stand for AS target genes. Larger node sizes indicate higher degree values. The top six compound nodes with the largest size and highest degree were quercetin (MOL000098, degree = 116), dihydrotanshinone I (MOL007101, degree = 76), pelargonidin (MOL007101, degree = 61), luteolin (MOL000006, degree = 55), guggulsterone (MOL001175, degree = 55) and β-sitosterol (MOL000358, degree = 53) (Table 2, Figure 3). The top eight gene nodes were PTGS2 (degree = 74), PTGS1 (degree = 43), RXRA (degree = 41), MCOA2 (degree = 38), SCM5A (degree

**Table 2** 108 Bioactive Compounds of HLXLD

| MOL ID | Compound | OB(%) | DL | Botanical Drug | Degree |
|---|---|---|---|---|---|
| MOL000098 | Quercetin | 46.43 | 0.28 | *Commiphora myrrha* | 116 |
| MOL007101 | Dihydrotanshinone I | 45.04 | 0.36 | *Salvia miltiorrhiza* | 76 |
| MOL001004 | Pelargonidin | 37.99 | 0.21 | *Commiphora myrrha* | 61 |
| MOL000006 | Luteolin | 36.16 | 0.25 | *Salvia miltiorrhiza* | 55 |
| MOL001175 | Guggulsterone | 42.45 | 0.44 | *Commiphora myrrha* | 55 |
| MOL000358 | β-sitosterol | 36.91 | 0.75 | *Angelica sinensis, Commiphora myrrha* | 53 |
| MOL001026 | Commiphora myrrha nol C | 39.96 | 0.58 | *Commiphora myrrha* | 52 |
| MOL000449 | Stigmasterol | 43.83 | 0.76 | *Angelica sinensis, Salvia miltiorrhiza* | 44 |
| MOL007122 | Miltirone | 38.76 | 0.25 | *Salvia miltiorrhiza* | 43 |
| MOL007077 | Sclareol | 43.67 | 0.21 | *Salvia miltiorrhiza* | 39 |
| MOL001263 | 3-oxo-tirucallic, acid | 42.86 | 0.81 | *Boswellia sacra* | 35 |
| MOL007154 | Tanshinone iia | 49.89 | 0.40 | *Salvia miltiorrhiza* | 34 |
| MOL002915 | Salvigenin | 49.07 | 0.33 | *Salvia miltiorrhiza* | 34 |
| MOL001659 | Poriferasterol | 43.83 | 0.76 | *Salvia miltiorrhiza* | 32 |
| MOL001093 | Cabraleone | 36.21 | 0.82 | *Commiphora myrrha* | 31 |
| MOL001215 | Tirucallol | 42.12 | 0.75 | *Boswellia sacra* | 31 |
| MOL007079 | Tanshinaldehyde | 52.47 | 0.45 | *Salvia miltiorrhiza* | 30 |
| MOL007081 | Danshenol B | 57.95 | 0.56 | *Salvia miltiorrhiza* | 30 |
| MOL007069 | Przewaquinone c | 55.74 | 0.40 | *Salvia miltiorrhiza* | 28 |
| MOL007125 | Neocryptotanshinone | 52.49 | 0.32 | *Salvia miltiorrhiza* | 28 |
| MOL002222 | Sugiol | 36.11 | 0.28 | *Salvia miltiorrhiza* | 26 |
| MOL001002 | Ellagic acid | 43.06 | 0.43 | *Commiphora myrrha* | 26 |
| MOL001956 | Cnidilin | 32.69 | 0.28 | *Angelica sinensis* | 25 |
| MOL001942 | Isoimperatorin | 45.46 | 0.23 | *Angelica sinensis, Salvia miltiorrhiza, Commiphora myrrha* | 25 |
| MOL007064 | Przewalskin b | 110.32 | 0.44 | *Salvia miltiorrhiza* | 24 |
| MOL007088 | Cryptotanshinone | 52.34 | 0.40 | *Salvia miltiorrhiza* | 23 |
| MOL005384 | Suchilactone | 57.52 | 0.56 | *Angelica sinensis* | 22 |
| MOL006812 | Phyllanthin | 33.31 | 0.42 | *Angelica sinensis* | 22 |
| MOL006824 | α-amyrin | 39.51 | 0.76 | *Salvia miltiorrhiza* | 22 |
| MOL007061 | Methylenetanshinquinone | 37.07 | 0.36 | *Salvia miltiorrhiza* | 22 |
| MOL007111 | Isotanshinone II | 49.92 | 0.40 | *Salvia miltiorrhiza* | 22 |

(*Continued*)

**Table 2** (Continued).

| MOL ID | Compound | OB(%) | DL | Botanical Drug | Degree |
|---|---|---|---|---|---|
| MOL001265 | Acetyl-alpha-boswellic, acid | 42.73 | 0.70 | *Boswellia sacra* | 22 |
| MOL002651 | Dehydrotanshinone II A | 43.76 | 0.40 | *Salvia miltiorrhiza* | 20 |
| MOL007041 | 2-isopropyl-8-methylphenanthrene-3,4-dione | 40.86 | 0.23 | *Salvia miltiorrhiza* | 20 |
| MOL007049 | 4-methylenemiltirone | 34.35 | 0.23 | *Salvia miltiorrhiza* | 20 |
| MOL001131 | Phellamurin_qt | 56.60 | 0.39 | *Commiphora myrrha* | 20 |
| MOL001771 | Poriferast-5-en-3beta-ol | 36.91 | 0.75 | *Salvia miltiorrhiza* | 19 |
| MOL007115 | Manool | 45.04 | 0.20 | *Salvia miltiorrhiza* | 19 |
| MOL001033 | Diayangambin | 63.84 | 0.81 | *Commiphora myrrha* | 19 |
| MOL008204 | Mono-O-methylwightin | 103.11 | 0.40 | *Salvia miltiorrhiza* | 18 |
| MOL007098 | Deoxyneocryptotanshinone | 49.40 | 0.29 | *Salvia miltiorrhiza* | 17 |
| MOL007124 | Neocryptotanshinone ii | 39.46 | 0.23 | *Salvia miltiorrhiza* | 17 |
| MOL007108 | Isocryptotanshi-none | 54.98 | 0.39 | *Salvia miltiorrhiza* | 16 |
| MOL007058 | Formyltanshinone | 73.44 | 0.42 | *Salvia miltiorrhiza* | 15 |
| MOL007093 | Dan-shexinkum d | 38.88 | 0.55 | *Salvia miltiorrhiza* | 15 |
| MOL001272 | INCENSOLE | 45.59 | 0.22 | *Boswellia sacra* | 15 |
| MOL007105 | Epidanshenspiroketallactone | 68.27 | 0.31 | *Salvia miltiorrhiza* | 14 |
| MOL007142 | Salvianolic acid j | 43.38 | 0.72 | *Salvia miltiorrhiza* | 14 |
| MOL008519 | Neotigogenin | 80.98 | 0.81 | *Salvia miltiorrhiza* | 14 |
| MOL007100 | Dihydrotanshinlactone | 38.68 | 0.32 | *Salvia miltiorrhiza* | 13 |
| MOL007145 | Salviolone | 31.72 | 0.24 | *Salvia miltiorrhiza* | 12 |
| MOL001987 | β-sitosterol | 33.94 | 0.70 | *Salvia miltiorrhiza* | 12 |
| MOL007119 | Miltionone I | 49.68 | 0.32 | *Salvia miltiorrhiza* | 11 |
| MOL007144 | Salviol | 31.72 | 0.24 | *Salvia miltiorrhiza* | 11 |
| MOL007050 | 2-(4-hydroxy-3-methoxyphenyl)-5-(3-hydroxypropyl)-7-methoxy-3-benzofurancarboxaldehyde | 62.78 | 0.40 | *Salvia miltiorrhiza* | 9 |
| MOL007094 | Danshenspiroketallactone | 50.43 | 0.31 | *Salvia miltiorrhiza* | 9 |
| MOL007156 | Tanshinone VI | 45.64 | 0.30 | *Salvia miltiorrhiza* | 9 |
| MOL007085 | Salvilenone | 30.38 | 0.38 | *Salvia miltiorrhiza* | 8 |
| MOL007118 | Microstegiol | 39.61 | 0.28 | *Salvia miltiorrhiza* | 8 |
| MOL007127 | 1-methyl-8,9-dihydro-7H-naphtho[5,6-g]benzofuran-6,10,11-trione | 34.72 | 0.37 | *Salvia miltiorrhiza* | 8 |
| MOL007130 | Prolithospermic acid | 64.37 | 0.31 | *Salvia miltiorrhiza* | 8 |
| MOL000490 | Petunidin | 30.05 | 0.31 | *Commiphora myrrha* | 8 |

(*Continued*)

**Table 2** (Continued).

| MOL ID | Compound | OB(%) | DL | Botanical Drug | Degree |
|---|---|---|---|---|---|
| MOL001601 | 1,2,5,6-tetrahydrotanshinone | 38.75 | 0.36 | *Salvia miltiorrhiza* | 7 |
| MOL001156 | 3-methoxyfuranoguaia-9- en-8-one | 35.15 | 0.18 | *Commiphora myrrha* | 7 |
| MOL007036 | 5,6-dihydroxy-7-isopropyl-1,1-dimethyl-2,3-dihydrophenanthren-4-one | 33.77 | 0.29 | *Salvia miltiorrhiza* | 6 |
| MOL007059 | 3-beta-Hydroxymethyllenetanshiquinone | 32.16 | 0.41 | *Salvia miltiorrhiza* | 6 |
| MOL007132 | (2R)-3-(3,4-dihydroxyphenyl)-2-[(Z)-3-(3,4-dihydroxyphenyl)acryloyl]oxy-propionic acid | 109.38 | 0.35 | *Salvia miltiorrhiza* | 6 |
| MOL001040 | (2R)-5,7-dihydroxy-2-(4-hydroxyphenyl)chroman-4-one | 42.36 | 0.21 | *Commiphora myrrha* | 6 |
| MOL002776 | Baicalin | 40.12 | 0.75 | *Salvia miltiorrhiza* | 5 |
| MOL007045 | 3α-hydroxytanshinone IIa | 44.93 | 0.44 | *Salvia miltiorrhiza* | 5 |
| MOL007068 | Przewaquinone B | 62.24 | 0.41 | *Salvia miltiorrhiza* | 5 |
| MOL007082 | Danshenol A | 56.97 | 0.52 | *Salvia miltiorrhiza* | 5 |
| MOL007121 | Miltipolone | 36.56 | 0.37 | *Salvia miltiorrhiza* | 5 |
| MOL007143 | Salvilenone I | 32.43 | 0.23 | *Salvia miltiorrhiza* | 5 |
| MOL007155 | (6S)-6-(hydroxymethyl)-1,6-dimethyl-8,9-dihydro-7H-naphtho[8,7-g] benzofuran-10,11-dione | 65.26 | 0.45 | *Salvia miltiorrhiza* | 5 |
| MOL000996 | Guggulsterol IV | 33.59 | 0.74 | *Commiphora myrrha* | 5 |
| MOL000569 | Digallate | 61.85 | 0.26 | *Salvia miltiorrhiza* | 4 |
| MOL007070 | (6S,7R)-6,7-dihydroxy-1,6-dimethyl-8,9-dihydro-7H-naphtho[8,7-g] benzofuran-10,11-dione | 41.31 | 0.45 | *Salvia miltiorrhiza* | 4 |
| MOL007120 | Miltionone II | 71.03 | 0.44 | *Salvia miltiorrhiza* | 4 |
| MOL007150 | (6S)-6-hydroxy-1-methyl-6-methylol-8,9-dihydro-7H-naphtho[8,7-g] benzofuran-10,11-quinone | 75.39 | 0.46 | *Salvia miltiorrhiza* | 4 |
| MOL007151 | Tanshindiol B | 42.67 | 0.45 | *Salvia miltiorrhiza* | 4 |
| MOL007152 | Przewaquinone E | 42.85 | 0.45 | *Salvia miltiorrhiza* | 4 |
| MOL001001 | Quercetin-3-O-β-D-glucuronide | 30.66 | 0.74 | *Commiphora myrrha* | 4 |
| MOL001126 | [(5aS,8aR,9R)-8-oxo-9-(3,4,5-trimethoxyphenyl)-5,5a,6,9-tetrahydroisobenzofurano[6,5-f][1,3] benzodioxol-8a-yl] acetate | 44.08 | 0.90 | *Commiphora myrrha* | 4 |
| MOL007048 | (E)-3-[2-(3,4-dihydroxyphenyl)-7-hydroxy-benzofuran-4-yl]acrylic acid | 48.24 | 0.31 | *Salvia miltiorrhiza* | 3 |
| MOL007071 | Przewaquinone f | 40.31 | 0.46 | *Salvia miltiorrhiza* | 3 |

(*Continued*)

**Table 2** (Continued).

| MOL ID | Compound | OB(%) | DL | Botanical Drug | Degree |
|---|---|---|---|---|---|
| MOL007107 | C09092 | 36.07 | 0.25 | *Salvia miltiorrhiza* | 3 |
| MOL001061 | (16S, 20R)-dihydroxydammar-24-en-3-one | 37.34 | 0.78 | *Commiphora myrrha* | 3 |
| MOL001062 | 15α-hydroxymansumbinone | 37.51 | 0.44 | *Commiphora myrrha* | 3 |
| MOL001138 | (3R,20S)-3,20-dihydroxydammar- 24-ene | 37.49 | 0.75 | *Commiphora myrrha* | 3 |
| MOL007063 | Przewalskin a | 37.11 | 0.65 | *Salvia miltiorrhiza* | 2 |
| MOL001006 | Poriferasta-7,22E-dien-3beta-ol | 42.98 | 0.76 | *Commiphora myrrha* | 2 |
| MOL001031 | Epimansumbinol | 61.81 | 0.40 | *Commiphora myrrha* | 2 |
| MOL001049 | 16-hydroperoxymansumbin-13(17)-en-3β-ol | 41.05 | 0.49 | *Commiphora myrrha* | 2 |
| MOL001063 | 28-acetoxy-15α-hydroxymansumbinone | 41.85 | 0.67 | *Commiphora myrrha* | 2 |
| MOL000988 | 4,17(20)-(cis)-pregnadiene-3,16-dione | 51.42 | 0.48 | *Commiphora myrrha* | 2 |
| MOL001243 | 3alpha-Hydroxy-olean-12-en-24-oic-acid | 39.32 | 0.75 | *Boswellia sacra* | 2 |
| MOL001255 | BOSWELLIC acid | 39.55 | 0.75 | *Boswellia sacra* | 2 |
| MOL004492 | chrysanthemaxanthin | 38.72 | 0.58 | *Angelica sinensis* | 1 |
| MOL007141 | Salvianolic acid g | 45.56 | 0.61 | *Salvia miltiorrhiza* | 1 |
| MOL010025 | Taraxanthin | 38.30 | 0.55 | *Salvia miltiorrhiza* | 1 |
| MOL001009 | Guggulsterol-VI | 54.72 | 0.43 | *Commiphora myrrha* | 1 |
| MOL001013 | Mansumbinoic acid | 48.10 | 0.32 | *Commiphora myrrha* | 1 |
| MOL001028 | (8R)-3-oxo-8-hydroxy-polypoda −13E,17E,21-triene | 44.83 | 0.59 | *Commiphora myrrha* | 1 |
| MOL001029 | Commiphora myrrha nones B | 34.39 | 0.67 | *Commiphora myrrha* | 1 |
| MOL001045 | (13E,17E,21E)-8-hydroxypolypodo-13,17,21-trien-3-one | 44.34 | 0.58 | *Commiphora myrrha* | 1 |
| MOL001095 | Isofouquierone | 40.95 | 0.78 | *Commiphora myrrha* | 1 |
| MOL001022 | 11α-hydroxypregna-4,17(20)-trans-diene-3,16-dione | 38.30 | 0.55 | *Commiphora myrrha* | 1 |

= 37), PTPN1 (degree = 37), HSP90AA1 (degree = 36) and ESR1 (degree = 34) (Figure 3). These top compounds and genes may be the critical nodes in the network and possess an important anti-AS effect.

## PPI Network Construction and Analysis

To obtain the PPI network from the STRING database, "Homo sapiens" was selected in the organism column, and the minimum required interaction score was set to 0.98 (Figure 4A). It contains 207 nodes and 405 edges, in which nodes represent protein names and edges represent protein interaction. To obtain the core PPI network, the initial PPI network

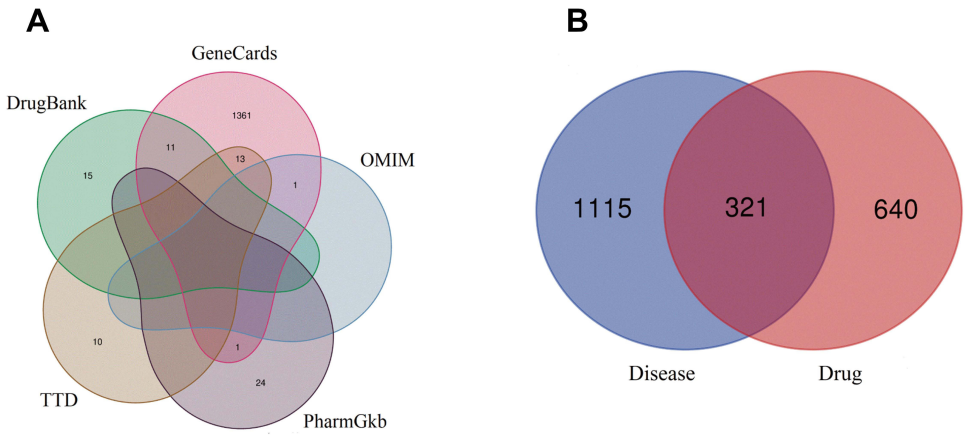


**Figure 2** Venn diagrams. (**A**) AS-related targets came from five databases. (**B**) The intersection genes of identified AS-related targets and targets of HLXLD.

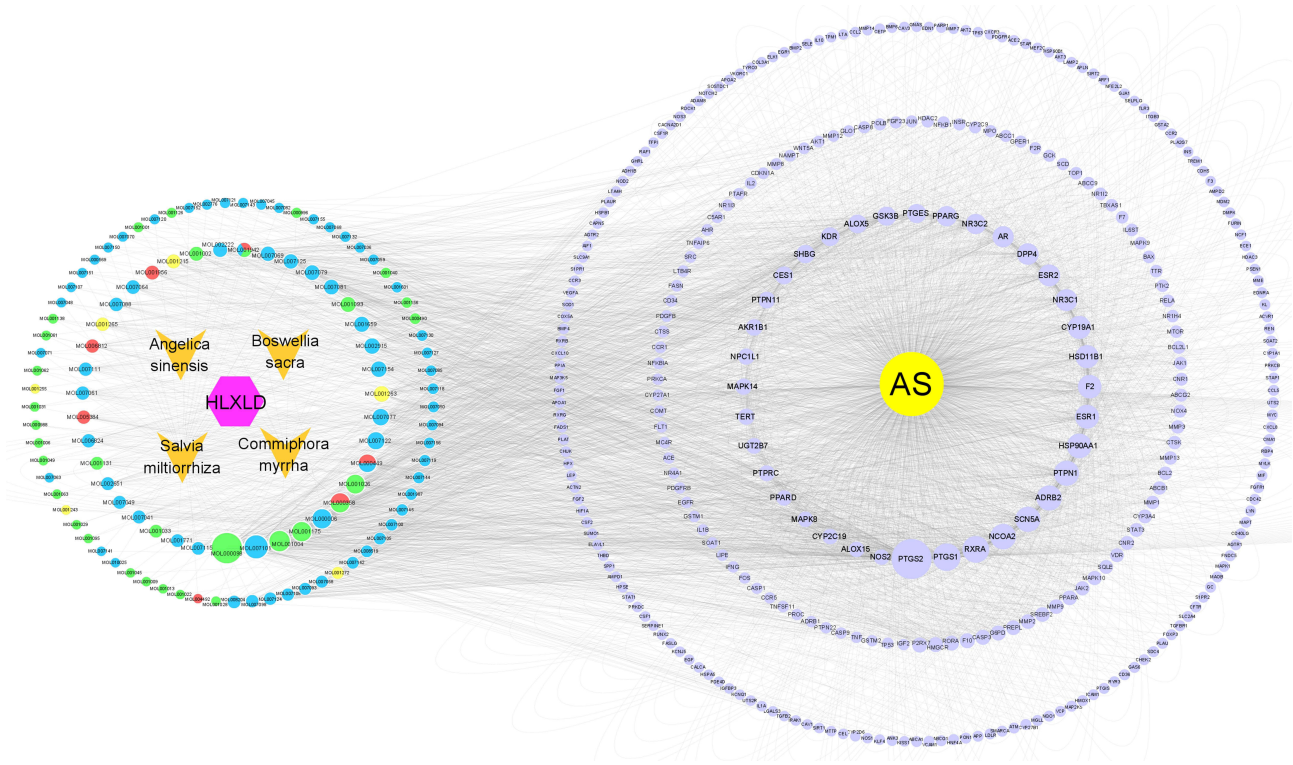


**Figure 3** C-D-T network of HLXLD in the treatment of AS. It contains 429 nodes and 1754 edges. The turmeric V nodes represent four botanical drugs from HLXLD. The circular nodes of red, blue, green and yellow stand for compounds from *Angelica sinensis, Salvia miltiorrhiza, Commiphora myrrha* and *Boswellia sacra*, respectively. The circular purple nodes stand for AS-related target genes. Larger node sizes indicate higher degree values.

was imported in Cytoscape 3.8.2 for visualization (Figure 4B). Then, the CytoNCA plugin was used to centrally analyze and evaluate the PPI network. In the first screening in Cytoscape 3.8.2, the selection criteria based on corresponding median values were set as follows: BC >8.27, CC >0.0236, DC >2.00, EC >0.01313, NC >0, and LAC >0. Only gene targets that met the criteria were retained and colored yellow in Figure 4B. After the first screening, the new network containing 66 nodes and 207 edges was retrieved (Figure 4C). Likewise, in the network in Figure 4C, only targets meeting the selection criteria (BC >467.16, CC >0.02395, DC >7.00, EC >0.07230, NC >0, and LAC >0) were retained and colored yellow in Figure 4C. After the second screening, the core PPI network with 16 nodes and 107 edges was

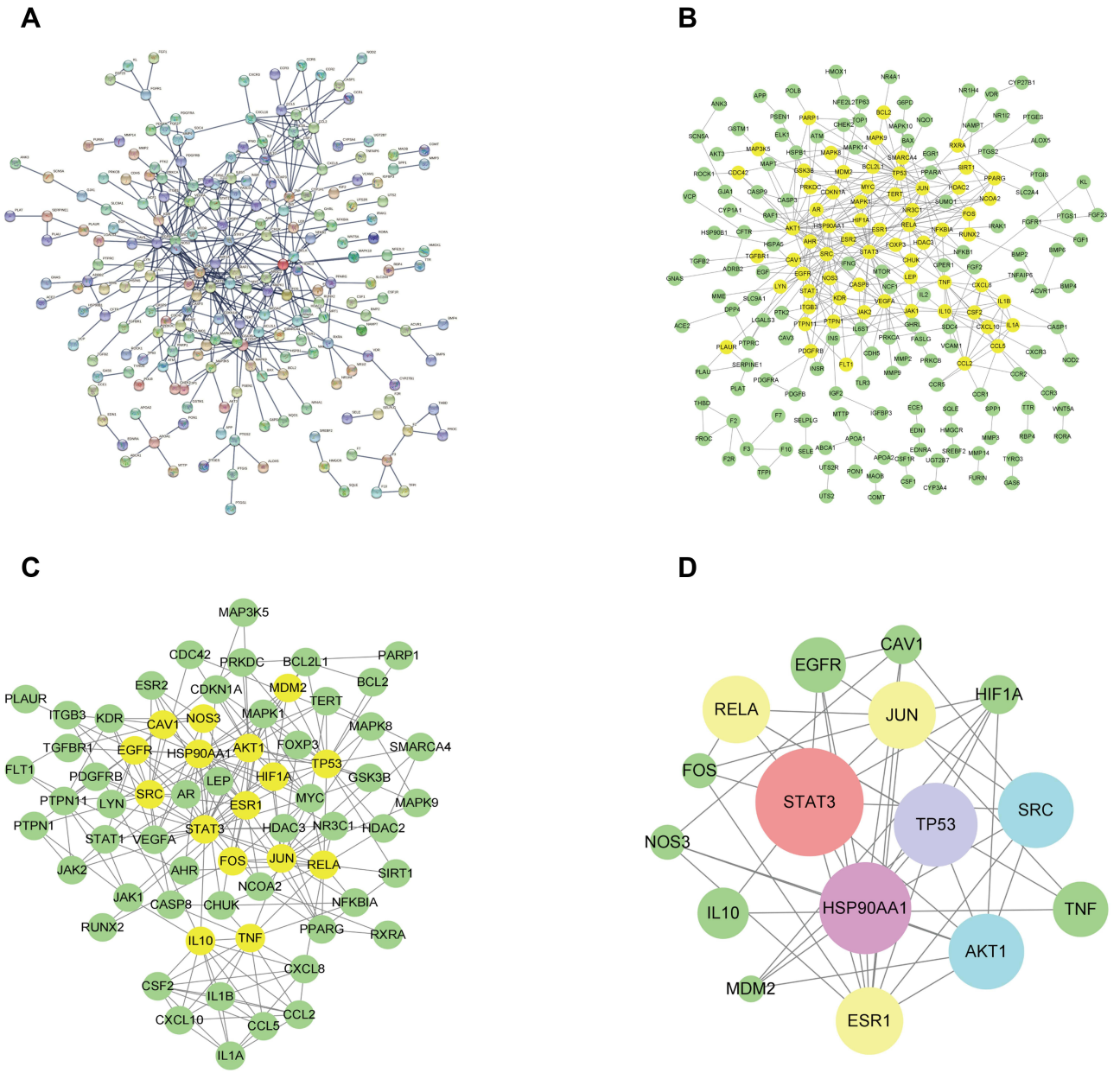


**Figure 4** PPI network of HLXLD-AS. (**A**) The interactive PPI network obtained from STRING database with species limited to "Homo sapiens", the minimum required interaction score set to 0.98, and the independent target protein nodes hidden. (**B**) Original PPI network from STRING database imported to Cytoscape 3.8.2 to obtain a new network. It contains 207 nodes and 405 edges. (**C**) PPI network screened from (**B**) in Cytoscape 3.8.2. It contains 66 nodes and 207 edges. (**D**) Core PPI network screened from (**C**) in Cytoscape 3.8.2. It contains 16 nodes and 107 edges. Larger node sizes indicate higher degree values.

obtained (Figure 2D). In the core PPI network, larger node sizes indicate higher degree values. The top eight target nodes were STAT3 (degree=25), HSP90AA1 (degree=21), TP53 (degree=19), AKT1 (degree=17), SRC (degree=17), RELA (degree=15), JUN (degree=15), and ESR1 (degree=15) (Figure 5), which may play a crucial role in the anti-AS effect of HLXLD.

## GO and KEGG Pathway Enrichment Analysis

A total of 321 common targets were input into R software to carry out GO and KEGG enrichment analysis. The GO enrichment analysis results were reflected in biological process (BP), cellular component (CC), and molecular function (MF). Under the condition of $P<0.05$ and $Q<0.05$, 3420, 108, and 293 items were obtained from these three aspects,

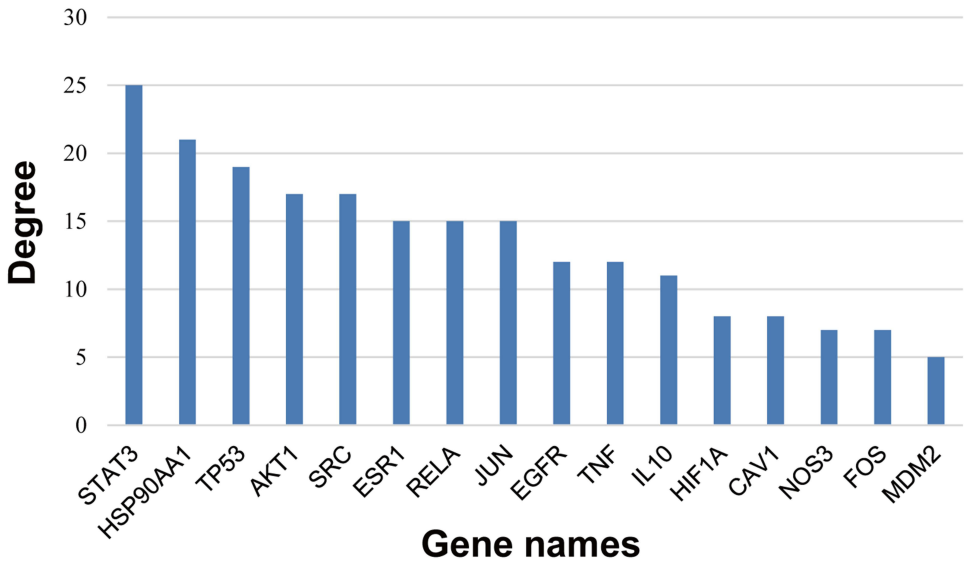


**Figure 5** The node degree distribution diagram of Figure 4D. The x-axis shows gene names and y-axis displays the degree value of related targets.

respectively. The top ten items of BP, CC, and MF were taken to make a visual bubble diagram with R software, as shown in Figure 6. The size of the dot indicates the number of genes contained under this entry. The color of the point represents the degree of enrichment, and the color from red to blue corresponds to the *Q* value from small to large. The top four entries of BP were enriched in response to molecule of bacterial origin (GO: 0002237), response to lipopolysaccharide (GO: 0032496), epithelial cell proliferation (GO: 0050673), and positive regulation of anion transport (GO: 1903793). The top four entries of CC were enriched in membrane raft (GO: 0045121), membrane microdomain (GO: 0098857), external side of plasma membrane (GO: 0009897), and focal adhesion (GO: 0005925). The top four entries of MF were enriched in signaling receptor activator activity (GO: 0030546), receptor ligand activity (GO: 0048018), DNA-binding transcription factor binding (GO: 0140297), and RNA polymerase II-specific DNA-binding transcription factor binding (GO: 0061629). The results showed that targets of HLXLD in the treatment of AS play a crucial role in BP, CC, and MF.

For 321 common targets of HLXLD in the treatment of AS, KEGG enrichment analysis was carried out with R software, and a total of 187 items were obtained (the results met $P<0.05$ and $Q<0.05$). The results ranked in the top 30 according to *Q* value were visualized (Figure 7). The size of the dot represents the number of genes contained under this entry, the color of the point represents the degree of enrichment, and the color from red to blue corresponds to the *Q* value from small to large. The top four pathways with the highest gene counts were lipid and atherosclerosis, fluid shear stress and atherosclerosis, MAPK signaling pathway, and PI3K-Akt signaling pathway. The detailed pathway map of the MAPK signaling pathway is drawn in Figure 8. To elucidate the interrelationships of 108 compounds, the C-P-T network containing 453 nodes and 2191 edges was constructed with the top 20 pathways and 321 target genes on a system (Figure 9) by Cytoscape 3.8.2, in which lipid and atherosclerosis pathway (degree = 62), fluid shear stress and atherosclerosis (degree = 53), MAPK signaling pathway (degree = 52) and PI3K-Akt signaling pathway (degree = 48) had higher gene counts. These findings indicates that HLXLD exerts a protective role in the treatment of AS through multi-pathways and multi-targets.

## Molecular Docking Analysis

A molecular docking strategy was used to study the interaction between ligand and receptor, and to predict the binding mode and affinity.[28] In the present study, candidate target proteins were selected for molecular docking analysis based on being from the human species and owning higher degree values in the core PPI network (Figure 4D). Candidate active compounds were selected for docking based on owning higher values of degree in the C-D-T network (Figure 3). Thus, the top eight candidate target proteins with the highest degree values (STAT3, PDB ID: 5AX3; HSP90AA1, PDB ID: 1UYD; TP53, PDB ID:2VUK; AKT1, PDB ID: 3O96; SRC, PDB ID:2H8H; RELA, PDB ID: 6YOW; ESR1, PDB ID: 1QKT; JUN, PDB ID: 1JUN) and six active compounds

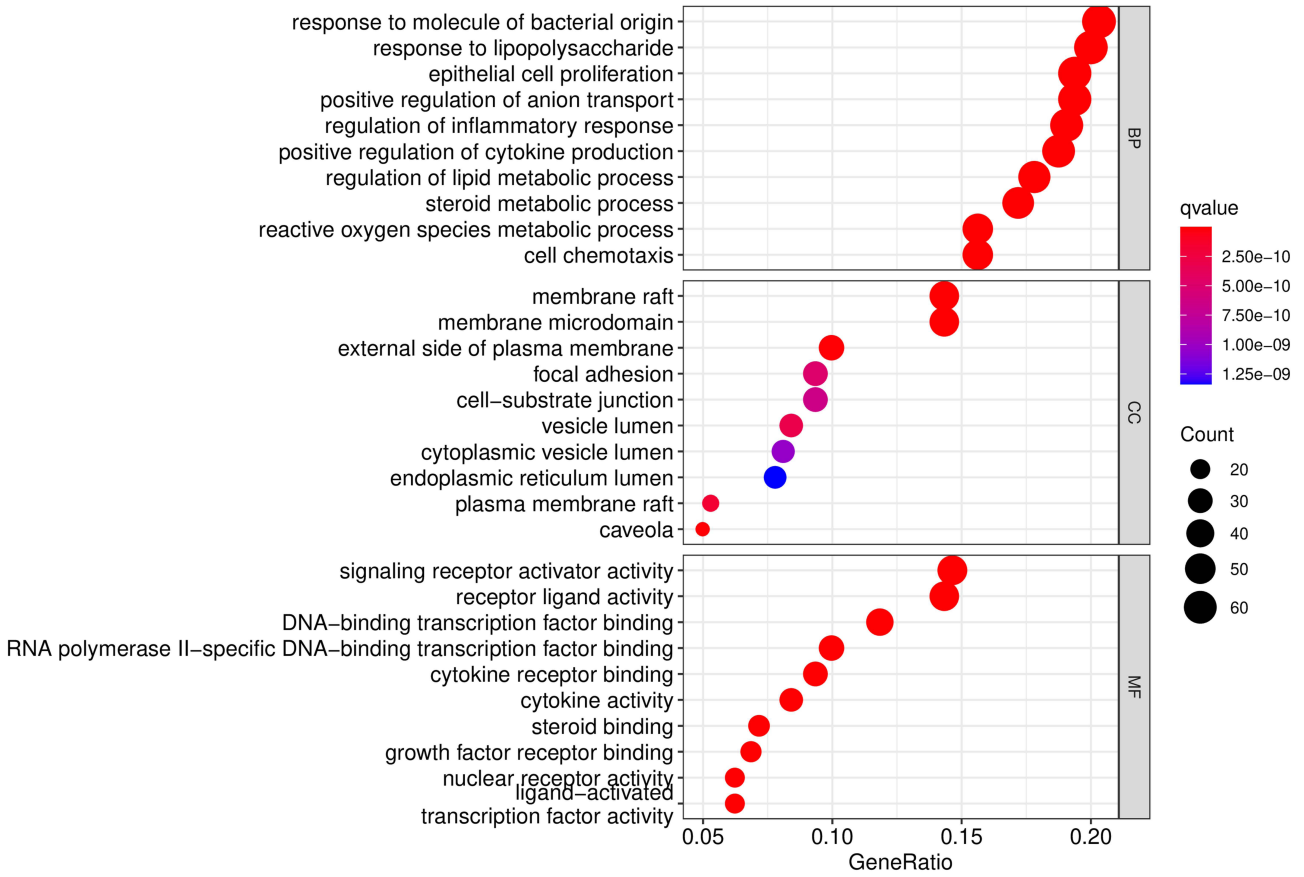


**Figure 6** The bubble diagram of GO enrichment analysis of HLXLD-AS genes. The top ten GO entries of BP, CC and MF were shown, respectively. The abscissa shows gene ratio and the ordinates displays enriched GO entries. The size of the dot is the number of genes contained under this entry, the color of the point represents the degree of enrichment and color from red to blue corresponds to *Q* value from small to large.

with degree >53 (Table 2, Figure 10) were chosen to conduct molecular docking (Table 3, Supplement Figure 1). According to the minimum binding energy, as shown in Table 3, STAT3-dihydrotanshinone I (−8.5 kcal/mol), HSP90AA1-dihydrotanshinone I (−10.1 kcal/mol), TP53-luteolin (−7.9 kcal/mol), AKT1-luteolin (−9.8 kcal/mol) were chosen to further analyze their binding mode, binding affinity and critical interaction by LigPlus 2.2 (2D) and Pymol 2.5 (3D) (Figure 11). According to Figure 11A-D, dihydrotanshinone I interacts with STAT3 by hydrogen bonds to Leu438(A) and Lys370(A) residues, hydrophobic bonds to Asp369(A), His437(A), Leu436(A), Val490(A), Asp371(A), Thr440(A) and His457(B) residues; dihydrotanshinone I interacts with HSP90AA1 by hydrophobic bonds to gly135(A), Leu107(A), Tyr139(A), Trp162(A), Phe138(A), Val150, Met98(A), Asn51 (A) residues; luteolin interacts with TP53 by hydrogen bonds to Ser99(A), Lys101(A), Gln100(A), Arg196(B), Ser166(A), Ala138(B) residues, hydrophobic bonds to Glu198(B), Met237(B), Asn235(B), Asp186(B), Gly199(B) and Leu201(B) residues; luteolin interacts with AKT1 by hydrogen bonds to Ser205(A), Thr211(A), Ile290(A), Gln79(A), Tyr272(A) residues, hydrophobic bonds to Trp80(A), Leu264(A), Val270(A), Asn54(A), Val271(A), Leu210(A) residues, respectively.

## Molecular Dynamics Simulation

Molecular dynamics simulation was used for studying the binding stability between the protein and the molecule. In the present study, STAT3-dihydrotanshinone I, HSP90AA1-dihydrotanshinone I, TP53-luteolin, and AKT1-luteolin were chosen to further analyze their binding stability. It can be seen from the RMSD graph (Figure 12): (1) The system of molecules and proteins is constantly fluctuating in the range of 0–10 ns during the kinetics process, indicating that the system is unstable and the protein is combined with their corresponding protein architecture when the phase changes constantly; (2) In the range of 10–100 ns, the RMSD value has been in a stable state, indicating that the binding between the protein and the molecule is extremely stable, and there is a good binding state between the two systems.

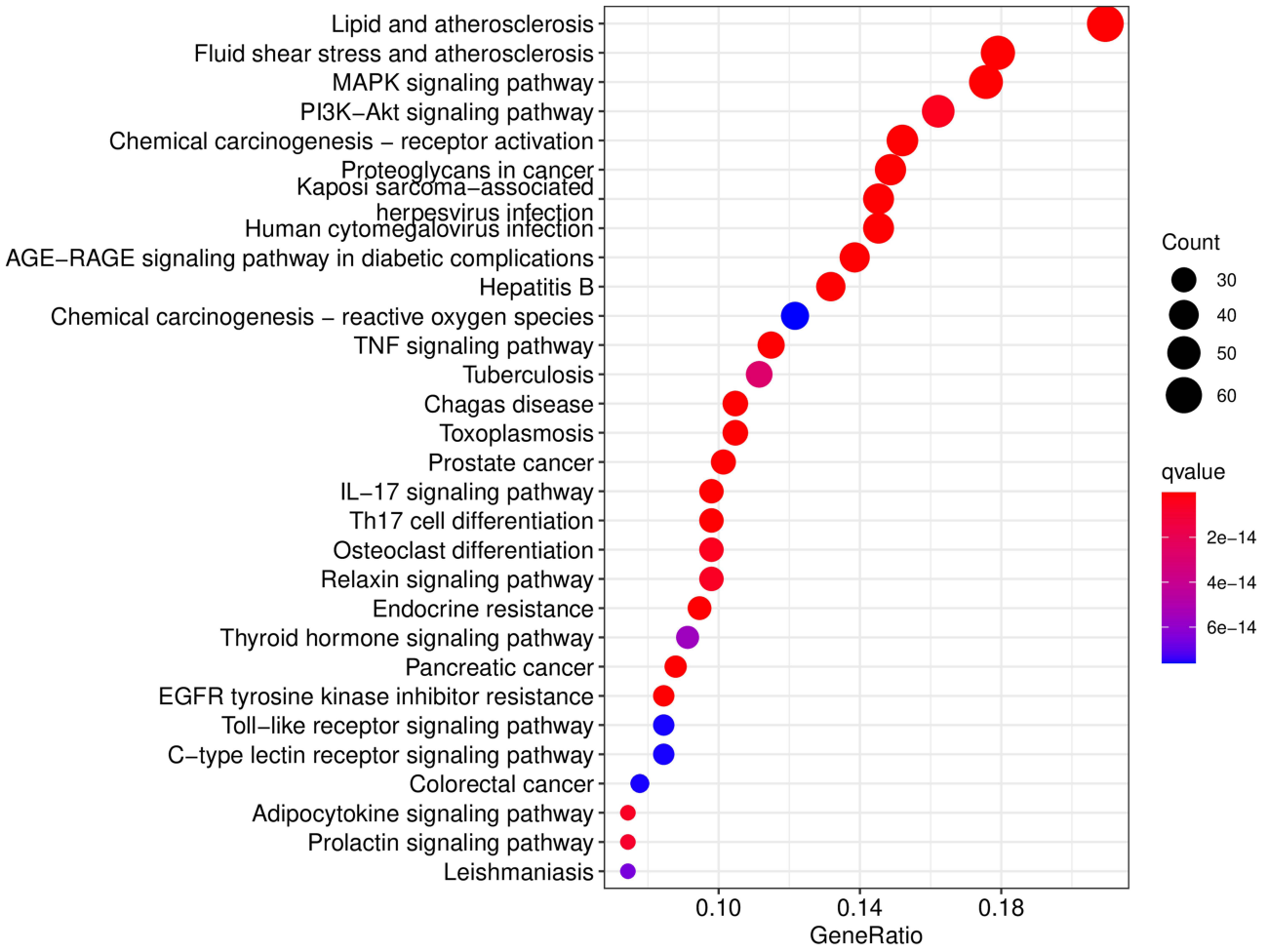


**Figure 7** The bubble diagram of KEGG enrichment pathway of HLXLD-AS genes. The top 30 pathways were shown. The abscissa shows gene ratio and the ordinates displays enriched GO entries. The size of the dot is the number of genes contained under this entry, the color of the point represents the degree of enrichment and the color from red to blue corresponds to *Q* value from small to large.

## Dihydrotanshinone I Suppressed the Accumulation of Lipid and Inflammation Induced by Ox-LDL in RAW264.7 Cells

The activation of macrophages, as indicated by lipid accumulation and increased inflammatory cytokines secretory, plays a key role in the pathological process of AS. In the present study, oil red O staining was employed to determine the intracellular lipid accumulation in RAW264.7 macrophage-derived foam cells. As shown in Figure 13A, there was a

**Table 3** Docking Binding Energy Results of Key Targets and Main Active Components (Kcal/Mol)

| Ligands | Receptors | | | | | | | |
|---|---|---|---|---|---|---|---|---|
| | STAT3 | HSP90AA1 | TP53 | AKT1 | SRC | ESR1 | RELA | JUN |
| Original ligands | −7.8 | −8.5 | −6.0 | −14.7 | −8.5 | −10.8 | −5.5 | −1.8 |
| Quercetin | / | −9.4 | −7.5 | −9.1 | / | | −7.6 | |
| Dihydrotanshinone I | −8.5 | −10.1 | / | / | −10.3 | −9.7 | −8.2 | |
| Pelargonidin | / | −9.6 | / | / | / | / | / | |
| Luteolin | / | −9.2 | −7.9 | −9.8 | / | | −7.8 | −5.5 |
| Guggulsterone | / | / | / | / | −9.4 | −8.5 | / | |
| β-sitosterol | / | −8.8 | / | −9.7 | / | −8.6 | / | −5.7 |

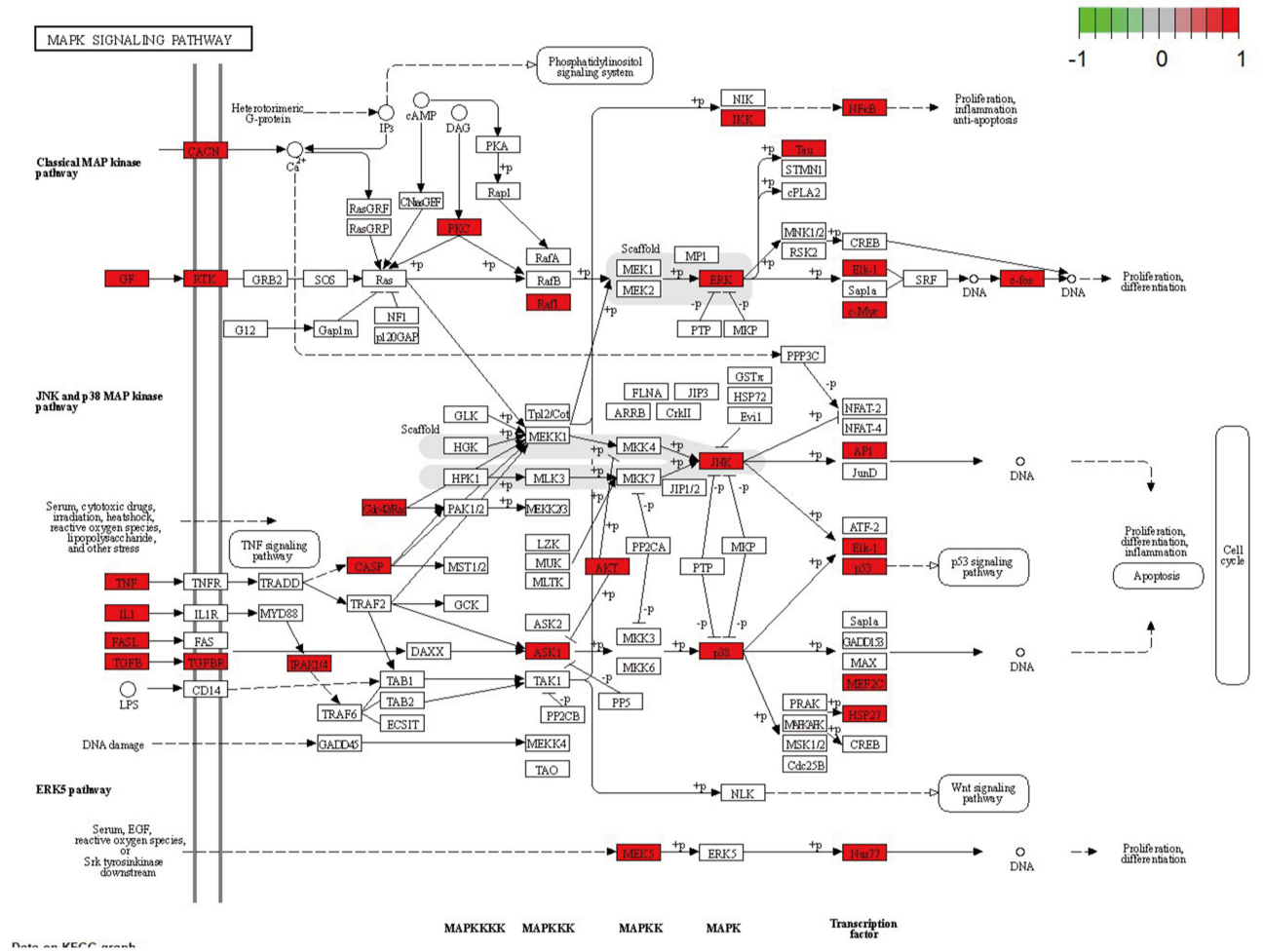


**Figure 8** The map of MAPK signaling pathway. There are 31 target genes (red color) enriched in MAPK signaling pathway.

large number of lipids accumulated in the ox-LDL group compared with the control (untreated) and dihydrotanshinone I groups, which means that the foam cells model was successfully induced by 50 μg/mL ox-LDL. Furthermore, the accumulation of lipids in ox-LDL-induced foam cells was decreased by the addition of dihydrotanshinone I in a dose-dependent manner. To investigate the anti-inflammatory effect of dihydrotanshinone I, we evaluated the secretory of several inflammatory cytokines in RAW264.7 cells using ELISA analyses. As shown in Figure 13B-D, the increased secretory of TNF-α, IL-1β, and MCP-1 induced by ox-LDL in RAW264.7 cells was significantly reduced by pretreating with dihydrotanshinone I.

## Dihydrotanshinone I Inhibited the STAT3 Phosphorylation and MAPK Signaling Pathway Activation in Ox-LDL-Treated RAW264.7 Cells

The results of network pharmacological analysis indicated that STAT3 is the key target and the MAPK signaling pathway is one of the important pathways of HLXLD against AS. To further verify the potential mechanism of dihydrotanshinone I in the treatment of AS, the phosphorylation of STAT3 and MAPK signaling key proteins (ERK, JNK, and p38) were determined. As shown in Figure 14, the phosphorylation expression of STAT3, ERK, JNK, and p38 were markedly increased in ox-LDL-treated RAW 264.7, whereas pretreating with dihydrotanshinone I can significantly inhibit the phosphorylation of STAT3, ERK, JNK, and p38. These results suggested that dihydrotanshinone I attenuated AS by inhibiting the activation of STAT3 and MAPK signaling pathways.

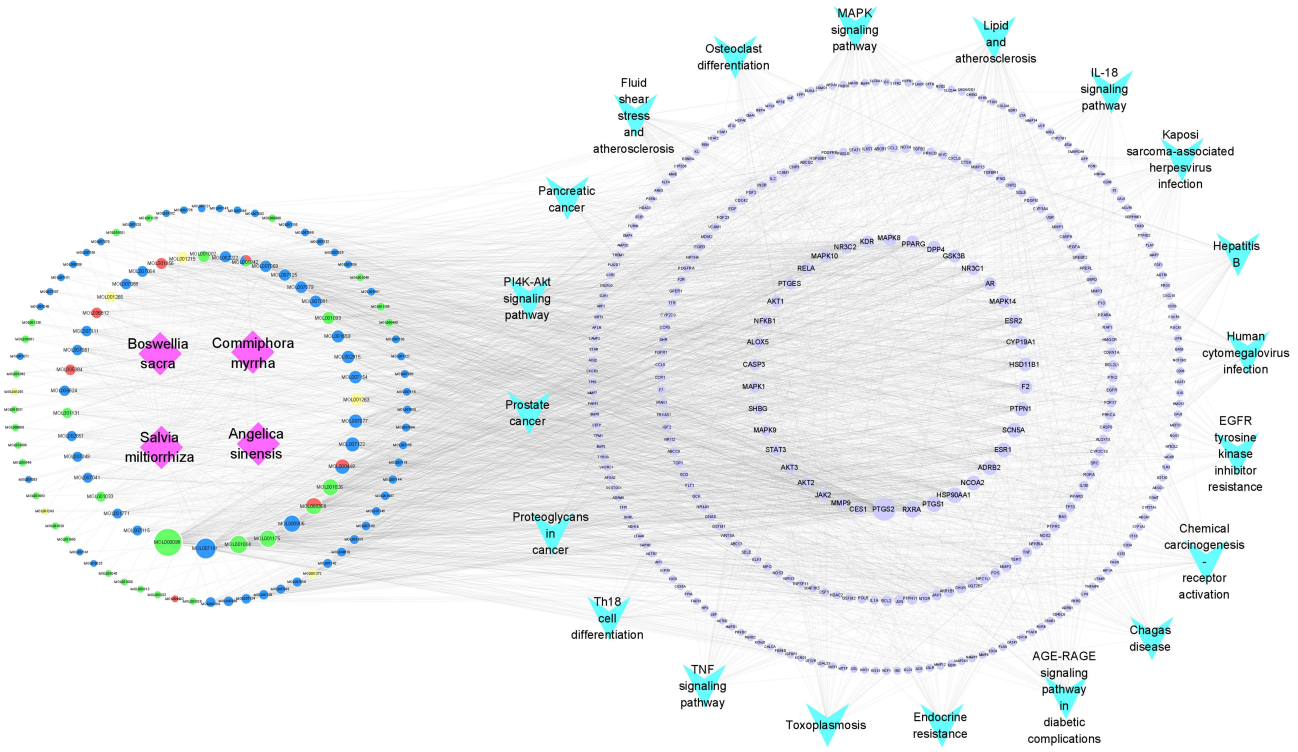


**Figure 9** C-P-T network of HLXLD in the treatment of AS. It contains 453 nodes and 2191 edges. The rose diamond nodes represent four botanical drugs from HLXLD. The circular nodes of red, blue, green and yellow stand for compounds from *Angelica sinensis, Salvia miltiorrhiza, Commiphora myrrha* and *Boswellia sacra*, respectively. The circular purple nodes stand for AS-related target genes. The light blue V nodes stand for the top 20 pathways in Figure 7. Larger node sizes indicate higher degree values.

## Discussion

TCM has been widely applied in treating multiple diseases in clinical practice in China. However, the underlying mechanism has not been easily elucidated clearly from the perspective of modern medicine for most of the TCM. The reason may lie in that the overall effect of TCM originates from the interaction between different components but is not limited to the superposition of single components.[30] In recent years, network pharmacology provides a new method that appropriately represents the overall diagnosis and treatment concepts for investigating the compatibility mechanism of TCM,[26] for example, the mechanism study of Spica Prunellae against thyroid-associated ophthalmopathy,[31] Bu Yang Huan Wu Decoction in the treatment of ischemic stroke,[32] and Liu Wei Di Huang Pill in treating type 2 diabetes mellitus.[33] Given the complex pathological mechanism of AS, more and more TCM with the characteristics of multiple targets are developed to treat AS. More importantly, the mechanism of several TCM against AS has been elucidated using network pharmacology. Zhang et al found that the Danshen-Shanzha herb-pair can target 41 proteins and 16 signal pathways related to inflammation, lipid metabolism, and endothelial protection in the treatment of AS.[15] Yeong et al screened 18 compounds in Gyejibokryeong-hwan and 213 AS-related targets, suggesting that the TNF, HIF-1, FoxO, and PI3K-Akt signal pathways mediate the beneficial effects of Gyejibokryeong-hwan on AS.[34]

HLXLD, a well-known traditional Chinese herbal prescription, possesses the ability to prevent AS, but its pharmacological mechanism has not been elucidated.[18,19] Those successful examples mentioned above in the application of TCM for treating AS inspired us to explore the mechanisms of HLXLD in AS by using network pharmacology analysis. The results of the present study showed that 108 active ingredients of HLXLD were found to act on 321 different targets associated with AS. According to the C-D-T network, quercetin, dihydrotanshinone I, pelargonidin, luteolin, guggulsterone, and β-sitosterol are highly connected with targets, which can be defined as vital compounds in HLXLD. Previous studies have determined that these compounds exhibit protective effects in the cardiovascular system,[23,35–39] indicating the beneficial effects of HLXLD in treating AS can be attributed to the combination of these core compounds.

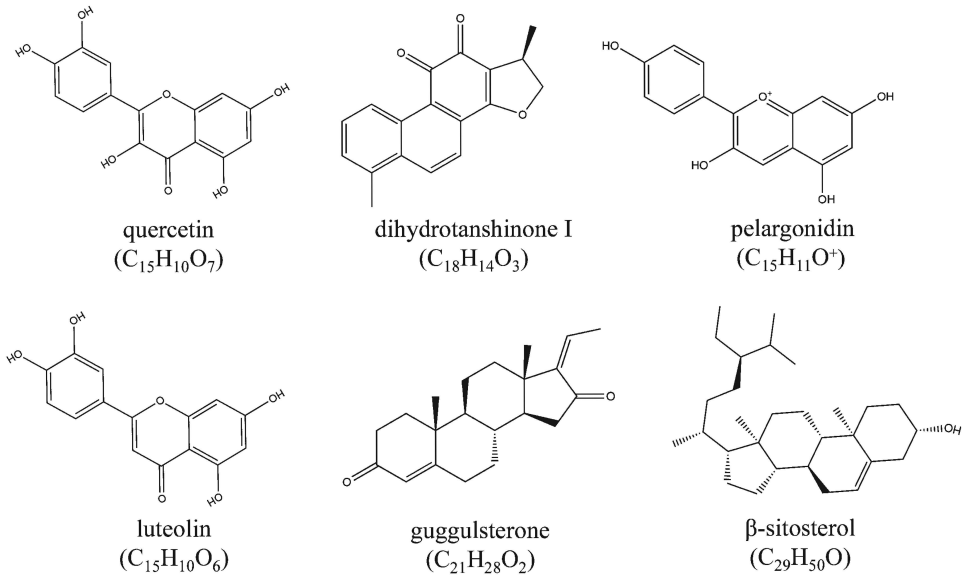


**Figure 10** The chemical structure and molecular formula of quercetin, dihydrotanshinone I, pelargonidin, luteolin, guggulsterone and β-sitosterol.

As far as each core active compound is concerned, quercetin, dihydrotanshinone I, pelargonidin, luteolin, guggulsterone, and β-sitosterol have been reported to possess excellent anti-AS effects. The mechanism of quercetin against AS involves gut metabolic regulation, enhancing autophagy and delaying senescence through the MST1 pathway.[20] Moreover, quercetin can restore the dysfunction of endothelial and lipid metabolism by regulating the ABCA1, LXR-α and PCSK9 expressions, and attenuating NADPH oxidase-dependent superoxide ($O^{2\cdot-}$) production.[40] Dihydrotanshinone I, whose mechanisms against AS involved in inhibiting LOX-1 mediated by NOX4/NF-κB signaling pathways, stabilizes vulnerable plaque by suppressing RIP3-mediated necroptosis of macrophage.[22,36] Besides quercetin and dihydrotanshinone I, pelargonidin exhibits potential preventive effects toward AS via inhibiting HASMC proliferation and migration.[37] Luteolin can treat AS through a variety of mechanisms including lipid metabolism renovation, inactivation of STAT3 and NLRP3 inflammasomes, macrophage polarization, as well as inhibition of AMPK-SIRT1 signaling pathway.[21,41] TMA/TMAO/FMO3 pathway mediates the protective effect of guggulsterone against AS.[39] Moreover, its antioxidant and anti-inflammatory activities may be another important mechanism.[23,42]

The main targets in the core PPI network, STAT3, HSP90AA1, TP53, and AKT1, play key roles in the occurrence and development of AS. STAT3, the protein node with the highest degree value in the core PPI network, is the signal transducer and activator of transcription 3 and plays an essential role in the process of AS including endothelial cell dysfunction, macrophage polarization, inflammation and immunity.[43] HSP90AA1, a heat shock protein, plays a protective role in the homeostasis of the vessel wall but has an impact on immunoinflammatory processes in pathological conditions involved in the development of AS.[44] P53 is a tumor suppressor protein, and the expression and transcriptional activity of P53 can be tightly regulated to treat AS.[45,46] AKT1, as a critical node in PI3K-PKB/Akt and pPI3K/Akt/mTOR signaling pathway, is involved in the progress and development of AS.[47,48]

Taken together, the above results showed that the core components and key targets of HLXLD in the C-D-T network play an important role in the treatment of AS. To integrate functions of 321 protein target genes, the GO enrichment analysis and KEGG pathway enrichment analysis were further conducted. GO results suggested that 321 target genes were enriched in BP, CC and MF, and mainly in BP. KEGG results suggested that 296 of the 321 target genes were enriched in 187 signal pathways, indicating a therapeutic effect of HLXLD on AS through multiple pathways. Among them, 62 of the 321 target genes enriched in lipid and atherosclerosis pathways, indicating lipid metabolism plays a pivotal role in the process of AS. Furthermore, research showed that the regulation of low-density lipoprotein (LDL) and cholesterol (LDL-C) is still the primary approach for the management and prevention of AS.[7] These findings are congruent with our view that lipid and atherosclerosis act as an important role in the anti-AS mechanism of HLXLD.

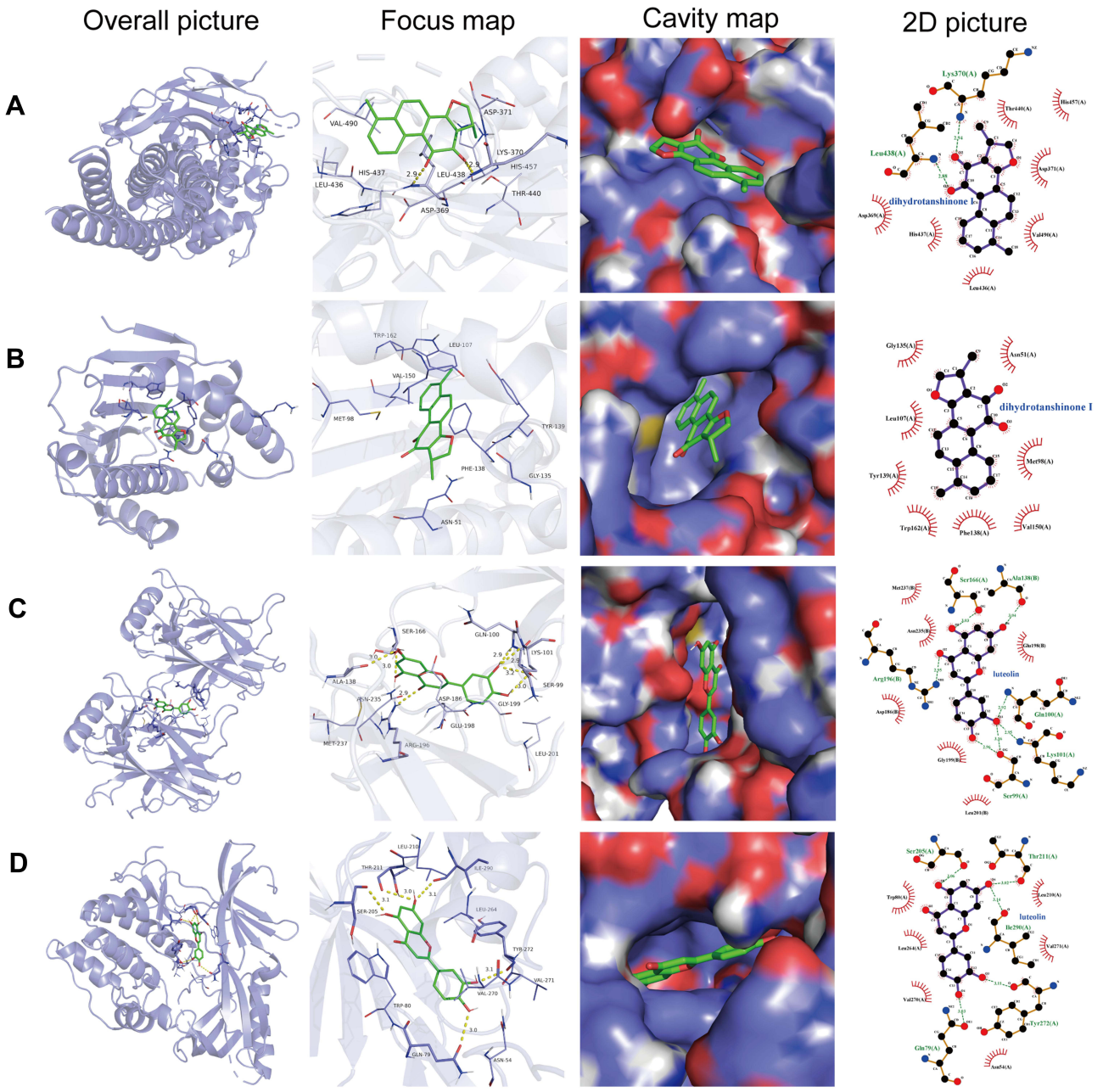


**Figure 11** The picture of molecule docking model. (**A-D**) Molecular docking of dihydrotanshinone I with STAT3, dihydrotanshinone I with HSP90AA1, luteolin with TP53 and luteolin with AKT1, respectively. The hydrogen bonds were represented by yellow dotted lines, and the length was marked around the lines.

In addition, MAPK and PI3K-AKT signaling pathways may be excellent therapeutic targets for HLXLD against AS. As one of the main information transmission pathways in cells, MAPK signaling pathway can regulate a variety of cell functions, such as proliferation, differentiation, transformation and death, and a series of inflammatory reactions in AS through activation.[49] For example, lncRNA VINAS regulates AS by modulating NF-κB and MAPK signaling.[50] The inhibition of microRNA-103 attenuates inflammation and endoplasmic reticulum stress in AS by disrupting the PTEN-mediated MAPK signaling.[51] Other studies have shown that TCM or TCM extract can regulate AS through the MAPK pathway, for instance, Tianxiangdan Granule alleviates atherosclerosis via p38 MAPK signaling pathways. Icariin attenuates high-cholesterol diet-induced AS in rats by preventing p38 MAPK signaling pathway.[52] PI3K-AKT pathway can participate in the regulation of AS by affecting macrophage polarization, lipid metabolism, autophagy and other

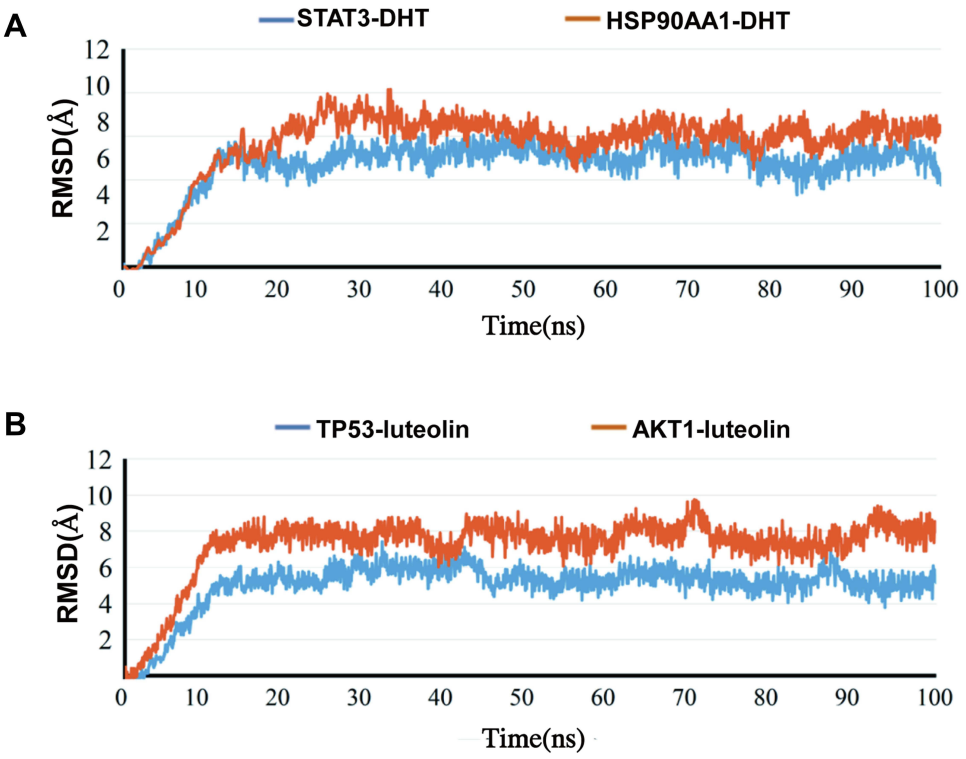


**Figure 12** The picture of RMSD value of molecular complex system in 100ns time interval. (**A**) The dynamic stability of dihydrotanshinone I with STAT3 (blue line) and with HSP90AA1 (red line). (**B**) The dynamic stability luteolin with TP53 (blue line) and with AKT1 (red line). DHT: dihydrotanshinone I.

functions,[53] which is a potential target for the treatment of AS. Wang et al suggested that nepsilon-carboxymethyl-lysine induces foam cell apoptosis in diabetic atherosclerosis by inhibiting the PI3K/AKT pathway.[54] Danhong Injection, a TCM preparation, attenuates high-fat-induced AS and macrophage lipid accumulation by regulating the PI3K/AKT Insulin Pathway.[53]

Numerous studies demonstrated that a TCM network pharmacology approach can clarify the interaction of multi-component to multi-target and multi-pathway. In this study, eight key target genes (STAT3, HSP90AA1, TP53, AKT1, SRC, RELA, ESR1and JUN) and four key pathways (lipid and atherosclerosis, fluid shear stress and atherosclerosis, MAPK signaling pathway, and PI3K-Akt signaling pathway) were regulated by three or more compounds in HLXLD. However, these findings were predicted by a network pharmacological approach and require further determination. Therefore, computer-aided prediction (molecular docking strategy) and experimental research verification (in vitro validation experiment) were conducted to further validate the prediction by network pharmacology analysis. Molecular docking results suggested that quercetin, dihydrotanshinone I, pelargonidin, luteolin, guggulsterone and β-sitosterol could be stably combined with their corresponding representative targets. In vitro experiments showed that the high phosphorylation levels of STAT3, ERK, JNK and p38 were reversed by dihydrotanshinone I, further validating the results of C-D-T network and KEGG. Previous research reports showed that mechanisms of dihydrotanshinone I against AS are involved in the inhibition of LOX-1 mediated by NOX4/NF-κB signaling pathways, and stabilizing vulnerable plaque by suppressing RIP3-mediated necroptosis of macrophage.[22,36] The present study determined that dihydrotanshinone I suppressed macrophage activation via inhibiting STAT3 and MAPK signaling pathways. Our results verify the new targets and pathways of dihydrotanshinone I in the treatment of AS.

However, the present study has several limitations based on the network pharmacology evaluation method guidance[55] and published literature.[56] Firstly, limited database usage. There are more TCM databases in addition to the several ones that we used to search for bioactive ingredients and potential targets, such as Traditional Chinese Medicine on Immuno-Oncology (TCMIO, http://tcmio.xielab.net/), SymMap v2 (http://www.symmap.org/) and Traditional Chinese Medicine Integrated Database (TCMID, https://ngdc.cncb.ac.cn/databasecommons/database/id/437). Secondly, the content of the

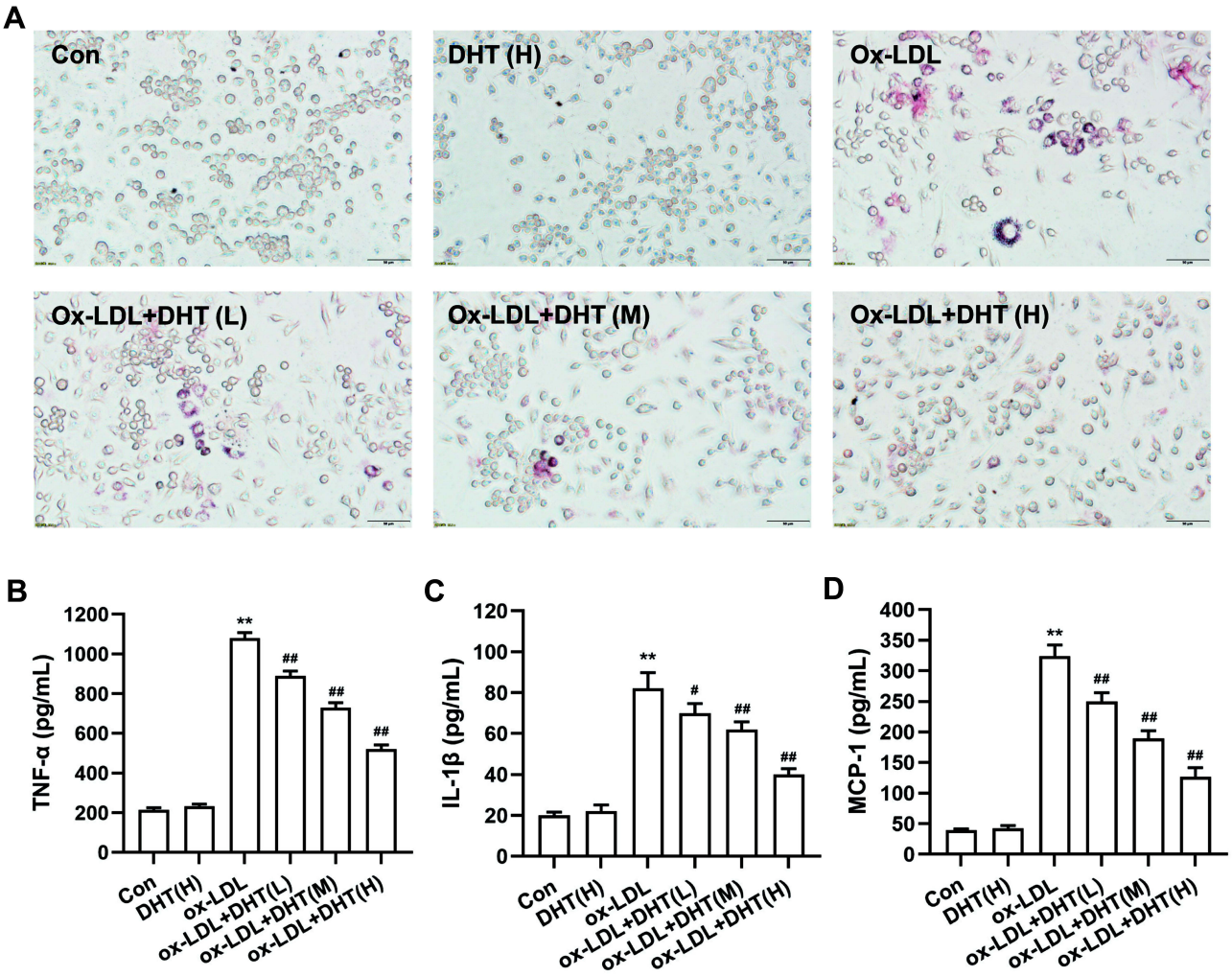


**Figure 13** The effect of dihydrotanshinone I on lipid accumulation and the secretory levels of inflammatory factor in ox-LDL-induced RAW264.7 cells. (**A**) Oil red O staining of RAW264.7 cells; (**B-D**) the effect of dihydrotanshinone I on the secretory levels of TNF-α, IL-1β, MCP-1, respectively. DHT: dihydrotanshinone I. Data are mean ±S.E.M. n=3. $^{**}P < 0.01$ vs Control; $^{\#}P < 0.05$, $^{\#\#}P < 0.01$ vs ox-LDL.

main bioactive ingredients is lacking. In the collection of chemical compounds of HLXLD, we conducted the study based on public databases, which lack relevant quantitative data. Probably, some of them may have only trace content and contribute little to the therapeutic effect of HLXLD. Therefore, future research on content determination should be carried out. Thirdly, the specifically binding relationship between active compounds and their targets was not verified. Molecular docking is a strategy to predict the combination of active compounds with core targets, rather than validate the network data. Therefore, more methods, such as Surface Plasmon Resonance (SPR) technology, can be used to validate whether active compounds bind specifically to their targets. Lastly, the validation experiment was insufficient. Dihydrotanshinone I, though determined as one of the most important bioactive ingredients of HLXLD against AS, could not completely stand for HLXLD. Thus, animal experiments and clinical research verification need to be further carried out to explore the potential molecular mechanism of HLXLD in treating AS.

In conclusion, we firstly utilized network pharmacology and molecular docking strategy to explore the underlying mechanism of HLXLD in treating AS. The main active components are quercetin, dihydrotanshinone I, pelargonidin, luteolin, guggulsterone and β-sitosterol, as well as key targets are STAT3, HSP90AA1, TP53, AKT1, SRC, RELA, ESR1 and JUN. The interaction between active components and targets is dominated by hydrophobic interaction. Additionally, the protective effect and underlying mechanism of dihydrotanshinone I on AS were validated by cell experiments. The

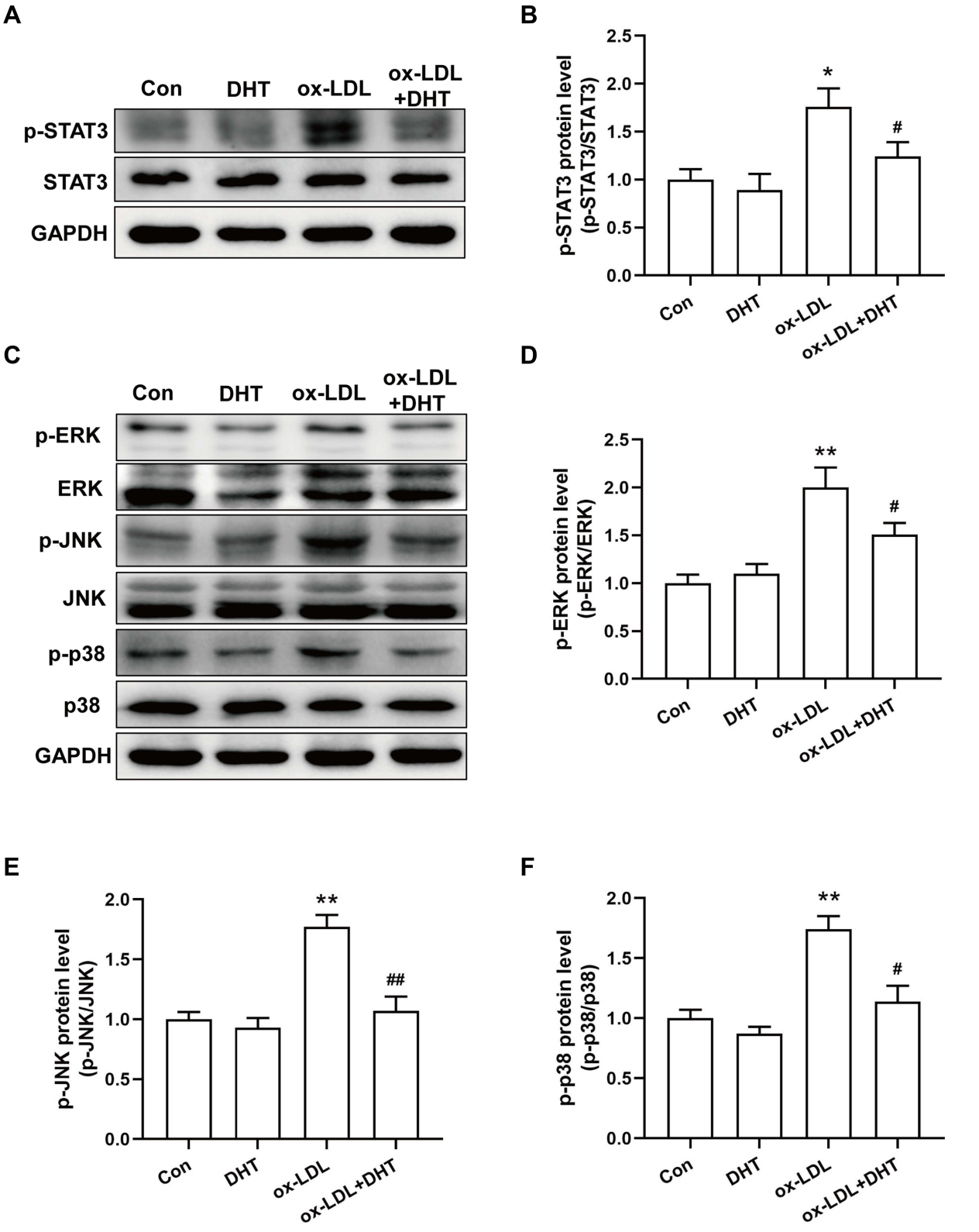


**Figure 14** The effect of dihydrotanshinone I on the protein secretion of p-STAT3 and MAPK signal pathway in ox-LDL-induced RAW264.7 cells. (**A**) Representative immunoblotting images of p-STAT3, STAT3 and GAPDH; (**C**) Representative immunoblotting images of p-ERK, ERK, p-JNK, JNK, p-p38, p38 and GAPDH; (**B, D-F**) Gray value statistics of corresponding proteins. DHT: dihydrotanshinone I. Data are mean±S.E.M. n=3. $^{**}P < 0.01$ vs Control; $^{\#}P < 0.05$, $^{\#\#}P < 0.01$ vs ox-LDL.

above results indicate that HLXLD is effective in the AS treatment through multi-component, multi-target and multi-pathway, which provides a scientific basis for explaining the detailed mechanism of HLXLD against AS.

## Acknowledgments

This work was supported by the National Natural Science Foundation of China (81600291); the key research and development projects of Hunan Provincial Science and Technology Department (2022SK2011); the science and technology innovation Program of Hunan Province (2021RC4064). This work was carried out in Hunan Key Laboratory of Vascular Biology and Translational Medicine.

## Disclosure

The authors declare no conflicts of interest in this work.

## References

1. Burnett JR, Hooper AJ, Hegele RA. Remnant Cholesterol and Atherosclerotic Cardiovascular Disease Risk. *J Am Coll Cardiol*. 2020;76(23):2736–2739. doi:10.1016/j.jacc.2020.10.029
2. Kamstrup PR. Lipoprotein(a) and Cardiovascular Disease. *Clin Chem*. 2021;67(1):154–166. doi:10.1093/clinchem/hvaa247
3. Zhao D, Liu J, Wang M, Zhang X, Zhou M. Epidemiology of cardiovascular disease in China: current features and implications. *Nat Rev Cardiol*. 2019;16(4):203–212. doi:10.1038/s41569-018-0119-4
4. Libby P, Buring JE, Badimon L, et al. Atherosclerosis. *Nat Rev Dis Primers*. 2019;5(1):56. doi:10.1038/s41572-019-0106-z
5. Capodanno D, Angiolillo DJ. Antithrombotic Therapy for Atherosclerotic Cardiovascular Disease Risk Mitigation in Patients With Coronary Artery Disease and Diabetes Mellitus. *Circulation*. 2020;142(22):2172–2188. doi:10.1161/CIRCULATIONAHA.120.045465
6. Ravnskov U, Alabdulgader A, de Lorgeril M, et al. The new European guidelines for prevention of cardiovascular disease are misleading. *Expert Rev Clin Pharmacol*. 2020;13(12):1289–1294. doi:10.1080/17512433.2020.1841635
7. Gupta M, Blumenthal C, Chatterjee S, et al. Novel emerging therapies in atherosclerosis targeting lipid metabolism. *Expert Opin Investig Drugs*. 2020;29(6):611–622. doi:10.1080/13543784.2020.1764937
8. Dai YJ, Wan SY, Gong SS, Liu JC, Li F, Kou JP. Recent advances of traditional Chinese medicine on the prevention and treatment of COVID-19. *Chin J Nat Med*. 2020;18(12):881–889. doi:10.1016/S1875-5364(20)60031-0
9. Pan X, Tao H, Nie M, et al. A clinical study of traditional Chinese medicine prolonging the survival of advanced gastric cancer patients by regulating the immunosuppressive cell population: a study protocol for a multicenter, randomized controlled trail. *Medicine*. 2020;99(16):e19757. doi:10.1097/MD.0000000000019757
10. Liu T, Ding Y, Wen A. Traditional Chinese medicine for ischaemic stroke. *Lancet Neurol*. 2018;17(9):745. doi:10.1016/S1474-4422(18)30290-4
11. Chai C, Hong F, Yan Y, et al. Effect of traditional Chinese medicine formula GeGen decoction on primary dysmenorrhea: a randomized controlled trial study. *J Ethnopharmacol*. 2020;261:113053. doi:10.1016/j.jep.2020.113053
12. Kou FS, Shi L, Li JX, et al. Clinical evaluation of traditional Chinese medicine on mild active ulcerative colitis: a multi-center, randomized, double-blind, controlled trial. *Medicine*. 2020;99(35):e21903. doi:10.1097/MD.0000000000021903
13. Wang C, Niimi M, Watanabe T, Wang Y, Liang J, Fan J. Treatment of atherosclerosis by traditional Chinese medicine: questions and quandaries. *Atherosclerosis*. 2018;277:136–144. doi:10.1016/j.atherosclerosis.2018.08.039
14. Upadya H, Prabhu S, Prasad A, Subramanian D, Gupta S, Goel A. A randomized, double blind, placebo controlled, multicenter clinical trial to assess the efficacy and safety of Emblica officinalis extract in patients with dyslipidemia. *BMC Complement Altern Med*. 2019;19(1):27. doi:10.1186/s12906-019-2430-y
15. Huang L, Wang J, Xu R, Liu Y, Liu Z. Regulatory effect of traditional Chinese medicine on gut microbiota in patients with atherosclerosis: a protocol for systematic review and meta-analysis. *Medicine*. 2020;99(50):e23730. doi:10.1097/MD.0000000000023730
16. Wang N, Zhao X, Huai J, et al. Arachidonic acid metabonomics study for understanding therapeutic mechanism of Huo Luo Xiao Ling Dan on rat model of rheumatoid arthritis. *J Ethnopharmacol*. 2018;217:205–211. doi:10.1016/j.jep.2018.02.027
17. Han XD, Zhou ZW, Yang W, et al. A computational and functional study elicits the ameliorating effect of the Chinese herbal formula Huo Luo Xiao Ling Dan on experimental ischemia-induced myocardial injury in rats via inhibition of apoptosis. *Drug Des Devel Ther*. 2015;9:1063–1102. doi:10.2147/DDDT.S76336
18. Fang Y, Liu G, Zhang Y. Effect of New Huo Luo Xiao Ling Dan on the TGF-β in ApoE Knock-out Mice with Early Atherosclerosis. *WORLD CHINESE MEDICINE*. 2016;11(10):2019–2100.
19. Li J, Zhou X, Zheng C, Lai L, Li L. Comparison of mechanisms and efficacies of five formulas for improving blood circulation and removing blood stasis. *Digital Chinese Medicine*. 2021;4(2):144–158. doi:10.1016/j.dcmed.2021.06.007
20. Cao H, Jia Q, Yan L, Chen C, Xing S, Shen D. Quercetin Suppresses the Progression of Atherosclerosis by Regulating MST1-Mediated Autophagy in ox-LDL-Induced RAW264.7 Macrophage Foam Cells. *Int J Mol Sci*. 2019;20(23):58.
21. Ding X, Zheng L, Yang B, Wang X, Ying Y. Luteolin Attenuates Atherosclerosis Via Modulating Signal Transducer And Activator Of Transcription 3-Mediated Inflammatory Response. *Drug Des Devel Ther*. 2019;13:3899–3911. doi:10.2147/DDDT.S207185
22. Zhao W, Li C, Zhang H, et al. Dihydrotanshinone I Attenuates Plaque Vulnerability in Apolipoprotein E-Deficient Mice: role of Receptor-Interacting Protein 3. *Antioxid Redox Signal*. 2021;34(5):351–363. doi:10.1089/ars.2019.7796
23. Koo HJ, Park HJ, Byeon HE, et al. Chinese yam extracts containing beta-sitosterol and ethyl linoleate protect against atherosclerosis in apolipoprotein E-deficient mice and inhibit muscular expression of VCAM-1 in vitro. *J Food Sci*. 2014;79(4):H719–29. doi:10.1111/1750-3841.12401

24. Wen J, Chang Y, Huo S, et al. Tanshinone IIA attenuates atherosclerosis via inhibiting NLRP3 inflammasome activation. J Med. 2020;13(1):910–932. doi:10.18632/aging.202202
25. Boezio B, Audouze K, Ducrot P, Taboureau O. Network-based Approaches in Pharmacology. *Mol Inform*. 2017;1:36.
26. Zhou Z, Chen B, Chen S, et al. Applications of Network Pharmacology in Traditional Chinese Medicine Research. *Evid Based Complement Alternat Med*. 2020;2020:1646905. doi:10.1155/2020/1646905
27. Chen G, Seukep AJ, Guo M. Recent Advances in Molecular Docking for the Research and Discovery of Potential Marine Drugs. *Mar Drugs*. 2020;18(11):548. doi:10.3390/md18110545
28. Torres PHM, Sodero ACR, Jofily P, Silva-Jr FP. Key Topics in Molecular Docking for Drug Design. *Int J Mol Sci*. 2019;20(18):587. doi:10.3390/ijms20184574
29. Liu J, Liu J, Tong X, et al. Network Pharmacology Prediction and Molecular Docking-Based Strategy to Discover the Potential Pharmacological Mechanism of Huai Hua San Against Ulcerative Colitis. *Drug Des Devel Ther*. 2021;15:3255–3276. doi:10.2147/DDDT.S319786
30. Li S, Zhang B. Traditional Chinese medicine network pharmacology: theory, methodology and application. *Chin J Nat Med*. 2013;11(2):110–120. doi:10.1016/S1875-5364(13)60037-0
31. Zhang Y, Li X, Guo C, Dong J, Liao L. Mechanisms of Spica Prunellae against thyroid-associated Ophthalmopathy based on network pharmacology and molecular docking. *BMC Complement Med Ther*. 2020;20(1):229. doi:10.1186/s12906-020-03022-2
32. Gao Q, Tian D, Han Z, et al. Network Pharmacology and Molecular Docking Analysis on Molecular Targets and Mechanisms of Buyang Huanwu Decoction in the Treatment of Ischemic Stroke. *Evid Based Complement Alternat Med*. 2021;2021:8815447. doi:10.1155/2021/8815447
33. He D, Huang JH, Zhang ZY, et al. A Network Pharmacology-Based Strategy For Predicting Active Ingredients And Potential Targets Of LiuWei DiHuang Pill In Treating Type 2 Diabetes Mellitus. *Drug Des Devel Ther*. 2019;13:3989–4005. doi:10.2147/DDDT.S216644
34. Lee AY, Lee JY, Chun JM. Exploring the Mechanism of Gyejibokryeong-hwan against Atherosclerosis Using Network Pharmacology and Molecular Docking. *Plants*. 2020;9(12):87. doi:10.3390/plants9121750
35. Dabeek WM, Marra MV. Dietary Quercetin and Kaempferol: bioavailability and Potential Cardiovascular-Related Bioactivity in Humans. *Nutrients*. 2019;11(10):87. doi:10.3390/nu11102288
36. Zhao W, Li C, Gao H, Wu Q, Shi J, Chen X. Dihydrotanshinone I Attenuates Atherosclerosis in ApoE-Deficient Mice: role of NOX4/NF-kappaB Mediated Lectin-Like Oxidized LDL Receptor-1 (LOX-1) of the Endothelium. *Front Pharmacol*. 2016;7:418. doi:10.3389/fphar.2016.00418
37. Son JE, Jeong H, Kim H, et al. Pelargonidin attenuates PDGF-BB-induced aortic smooth muscle cell proliferation and migration by direct inhibition of focal adhesion kinase. *Biochem Pharmacol*. 2014;89(2):236–245. doi:10.1016/j.bcp.2014.02.015
38. Bu-Chun Zhang ZL, Xu W, Chu-Han X. Yan-Feng Ma Luteolin alleviates NLRP3 inflammasome activation and directs macrophage polarization in lipopolysaccharide-stimulated RAW264.7 cells. *Am J Transl Res*. 2018;10(1):265–273.
39. Gautam A, Paudel YN, Abidin S, Bhandari U. Guggulsterone, a farnesoid X receptor antagonist lowers plasma trimethylamine-N-oxide levels: an evidence from in vitro and in vivo studies. *Hum Exp Toxicol*. 2019;38(3):356–370. doi:10.1177/0960327118817862
40. Li SS, Cao H, Shen DZ, et al. Effect of Quercetin on Atherosclerosis Based on Expressions of ABCA1, LXR-alpha and PCSK9 in ApoE(-/-) Mice. *Chin J Integr Med*. 2020;26(2):114–121. doi:10.1007/s11655-019-2942-9
41. Zhang BC, Li Z, Xu W, Xiang CH, Ma YF. Luteolin alleviates NLRP3 inflammasome activation and directs macrophage polarization in lipopolysaccharide-stimulated RAW264.7 cells. *Am J Transl Res*. 2018;10(1):265–273.
42. Rosenblat M, Volkova N, Aviram M. Pomegranate phytosterol (beta-sitosterol) and polyphenolic antioxidant (punicalagin) addition to statin, significantly protected against macrophage foam cells formation. *Atherosclerosis*. 2013;226(1):110–117. doi:10.1016/j.atherosclerosis.2012.10.054
43. Chen Q, Lv J, Yang W, et al. Targeted inhibition of STAT3 as a potential treatment strategy for atherosclerosis. *Theranostics*. 2019;9(22):6424–6442. doi:10.7150/thno.35528
44. Xu Q, Metzler B, Jahangiri M, Mandal K. Molecular chaperones and heat shock proteins in atherosclerosis. *Am J Physiol Heart Circ Physiol*. 2012;302(3):H506–14. doi:10.1152/ajpheart.00646.2011
45. Wu G, Cai J, Han Y, et al. LincRNA-p21 regulates neointima formation, vascular smooth muscle cell proliferation, apoptosis, and atherosclerosis by enhancing p53 activity. *Circulation*. 2014;130(17):1452–1465. doi:10.1161/CIRCULATIONAHA.114.011675
46. Guevara NV, Kim HS, Antonova EI, Chan L. The absence of p53 accelerates atherosclerosis by increasing cell proliferation in vivo. *Nat Med*. 1999;5(3):335–339. doi:10.1038/6585
47. Chen L, Zheng SY, Yang CQ, Ma BM, Jiang D. MiR-155-5p inhibits the proliferation and migration of VSMCs and HUVECs in atherosclerosis by targeting AKT1. *Eur Rev Med Pharmacol Sci*. 2019;23(5):2223–2233. doi:10.26355/eurrev_201903_17270
48. Abeyrathna P, Su Y. The critical role of Akt in cardiovascular function. *Vascul Pharmacol*. 2015;74:38–48. doi:10.1016/j.vph.2015.05.008
49. Cheng M, Yang L, Fan M, An S, Li J. Proatherogenic stimuli induce HuR in atherosclerosis through MAPK/ErK pathway. *Am J Transl Res*. 2019;11(4):2317–2327.
50. Simion V, Zhou H, Pierce JB, et al. LncRNA VINAS regulates atherosclerosis by modulating NF-kappaB and MAPK signaling. *JCI Insight*. 2020;5(21):89. doi:10.1172/jci.insight.140627
51. Jiang L, Qiao Y, Wang Z, Ma X, Wang H, Li J. Inhibition of microRNA-103 attenuates inflammation and endoplasmic reticulum stress in atherosclerosis through disrupting the PTEN-mediated MAPK signaling. *J Cell Physiol*. 2020;235(1):380–393. doi:10.1002/jcp.28979
52. Sun LF, An DQ, Niyazi GL, Ma WH, Xu ZW, Xie Y. Effects of Tianxiangdan Granule treatment on atherosclerosis via NFkappaB and p38 MAPK signaling pathways. *Mol Med Rep*. 2018;17(1):1642–1650. doi:10.3892/mmr.2017.8067
53. Zhou M, Ren P, Li S, et al. Danhong Injection Attenuates High-Fat-Induced Atherosclerosis and Macrophage Lipid Accumulation by Regulating the PI3K/AKT Insulin Pathway. *J Cardiovasc Pharmacol*. 2019;74(2):152–161. doi:10.1097/FJC.0000000000000691
54. Wang Z, Bao Z, Ding Y, et al. Nepsilon-carboxymethyl-lysine-induced PI3K/Akt signaling inhibition promotes foam cell apoptosis and atherosclerosis progression. *Biomed Pharmacother*. 2019;115:108880. doi:10.1016/j.biopha.2019.108880
55. Li S. Network pharmacology evaluation method guidance-draft. *World J Tradit Chin Med*. 2021;7(1):146–154.
56. Liu Z, Cai C, Du J, et al. TCMIO: a Comprehensive Database of Traditional Chinese Medicine on Immuno-Oncology. *Front Pharmacol*. 2020;11:439. doi:10.3389/fphar.2020.00439